

# 学位論文

(Coumarine-4yl)methyl and Indenyl Cations: Case Studies of  
Triplet Ground State Cations

(4-クマリニルメチルカチオンとインデニルカチオン：  
三重項を基底状態に有するカルボカチオンの事例研究)

学位取得年月 2024年3月

広島大学先進理工系科学研究科

先進理工系科学専攻

基礎化学プログラム

高野 真綾



## Table of Contents

### 1. 主論文

(Coumarine-4yl)methyl and Indenyl Cations: Case Studies of Triplet Ground State Cations

(4-クマリニルメチルカチオンとインデニルカチオン：三重項を基底状態に有するカルボカチオンの事例研究)

### 2. 公表論文

(1) “Photoreaction of 4-(Bromomethyl)-7-(diethylamino)coumarin: Generation of a Radical and Cation Triplet Diradical during the C-Br Bond Cleavage”

Ma-aya Takano and Manabu Abe\*

*Organic Letter.* **2022**, *24*, 2804-2808.

(2) “Substituent Effects on the Electronic Ground State (Singlet versus Triplet) of Indenyl Cations: DFT and CASPT2 Studies

Ma-aya Takano, Ivana Antol and Manabu Abe\*

*European Journal of Organic Chemistry.* **2024**, doi; 10.1002/ejoc.202301226

# 主論文



**(Coumarine-4yl)methyl and Indenyl Cations: Case  
Studies of Triplet Ground State Cations**

March, 2024

Department of Chemistry,  
Graduate School of Advanced Science and Engineering,  
Hiroshima University

Ma-aya Takano



## Contents

### Chapter 1. General Introduction

1-1.	Reactive Intermediate.....	11
1-2.	Carbocations.....	11
1-3.	Triplet ground state ions.....	13
1-4.	Purpose of this research.....	16

### Chapter 2. Experimental Proof of Triplet Ground State Carbocation; (7-diethylaminocoumarin -4-yl)methyl cation

2-1.	Introduction.....	19
2-2.	Synthesis and absorption spectrum measurement of DEACM-Br.....	19
2-3.	Low-temperature IR and EPR measurements.....	20
2-4.	LFP measurements.....	23
2-5.	Product analysis of DEACM-Br.....	26
2-6.	Product analysis of DEACM-Br in the presence of 2,2,6,6-tetramethylpiperidine-1-oxyl (TEMPO) .....	28
2-7.	Mechanism.....	30
2-8.	Conclusion.....	31
2-9.	Experimental Section.....	32

### Chapter 3. Design of Triplet Ground State Indenyl Cation; Investigation of Substituent Effects

3-1.	Introduction.....	52
3-2.	Electronic structure and configuration of 7-17.....	53
3-3.	Singlet-Triplet energy splitting.....	54
3-4.	Quantitative evaluation of the substituent effect.....	56
3-5.	Nucleus-independent chemical shift (NICS) values (NICS(1) <sub>zz</sub> ) .....	58
3-6.	NBO charges and NBO spin densities.....	59
3-7.	Conclusion.....	60
3-8.	Supplementary information.....	61



## **Chapter 4. Conclusions and Outlook**

**Reference**

**List of Publications**

**Acknowledgements**

# **Chapter 1**

## **General Information**

## 1-1. Reactive Intermediate

To get desired products through chemical reactions, a deep understanding of the reaction mechanism is important. In the chemical reaction that generates reaction intermediates between reactants to products, its physical properties and structure are key to elucidating the reaction mechanism because its behavior dominates the reaction.

Moderately, research methods of reaction intermediates have been shifted from product-driven methods to accurate identification based on precise simulation of its physical properties or direct observation concomitant with progress of theoretical calculations and spectroscopic techniques<sup>1</sup>. Specifically, density functional theory (DFT) or complete active space multiconfiguration second perturbation theory (CASPT2) and laser flash photolysis (LFP), randomly interleaved pulse train (RIPT), pump-probe methods or matrix-isolation technics in theoretical calculations and spectroscopic, respectively. The development of these research methods has enabled today's researchers to gain a detail understanding of predicting and demonstrating novel reactivity of reaction intermediates, and even clarify their dynamics.

## 1.2 Carbocations

Carbocation is positively charged carbon species and one of the important reactive intermediates in organic chemistry which generates in heterolytic bond cleavage between carbon and heteronuclear atoms. Historically, in 1901, the existence of relatively stable carbocation such as triphenylmethyl cation was indicated by the independent reports by Norris<sup>2</sup>, Kehrman and Wentzel<sup>3</sup> that color changing of triphenylmethyl alcohol by addition of sulfuric acid. However, for a long time afterwards, its importance in chemistry was not recognized, and even its existence itself was doubted. The existence and importance of carbocations had been gradually recognized since pioneering work about S<sub>N</sub>1 and E1 reactions by Hans Meerwine, Christopher Ingold, Frank Whitmore *et al.* in 1920-1930s. Furthermore, in 1960s, Olah reported isolation technic by using SbF<sub>5</sub>/SOFSO<sub>3</sub>H-SbF<sub>5</sub> (magic acid)<sup>4</sup>, which accelerated the research about its

structure by NMR or IR. Recently, the structure analysis was accomplished by single crystal X-ray analysis<sup>5-8</sup>, and it indicates great interest in carbocation chemistry. Since the 1980s, many attempts were made to observe carbocations generated by photoreaction by LFP method<sup>9</sup>, which indicates the importance of carbocations as reactive intermediate not only in thermal reaction but also in photoreaction.

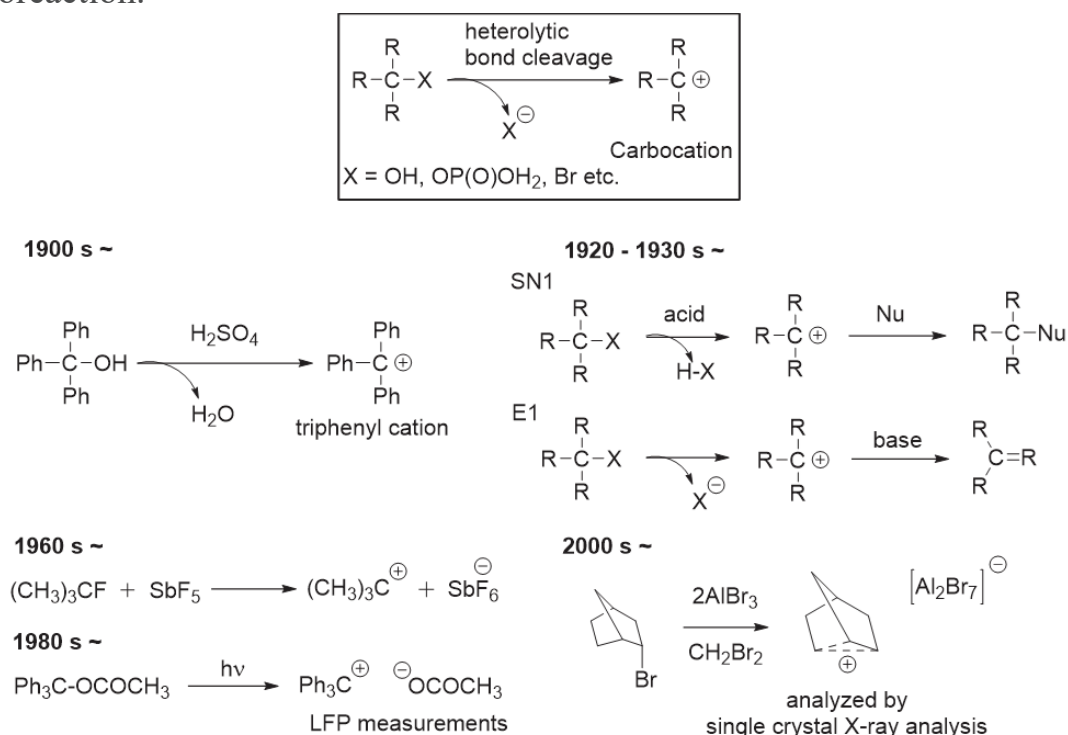


**Figure 1.** Historical context of carbocation chemistry.

Although carbocation has been intensively studied by many chemists for more than 100 years, its electronic structure was not so actively discussed. 2 reasons can be considered. 1) Because carbocations have vacant p orbital (or sp<sup>2</sup>) but don't have lone-pair, electronic structure except for closed-shell singlet has not been anticipated. 2) The report that the triplet state of methyl cation is 90 kcal mol<sup>-1</sup> more unstable than the singlet state indicated by theoretical calculation in 1982 by People<sup>10</sup> discourages the consideration of other electronic states. Recently, however, advances in theoretical calculations have led to the proposal of the existence of triplet ground state carbocations because of the substituent effects, opening a new dimension in carbocation chemistry.

### 1-3. Triplet ground state ions

Recently, the switching of the electronic ground state of ionic reactive intermediate including carbocation by substituent effect has been studied with theoretical calculation and experimental approaches. In the carbocation case, because it doesn't have a lone pair, a triplet ground state will be accomplished with electron-rich substituents.

The first example of such triplet ground state carbocation is phenyl cation. Phenyl cation which can be generated by the photoreaction of benzene diazonium salts or chlorobenzene, has a vacant  $sp^2$  orbital in its singlet state, and the non-substituted one is singlet ground state. However, when introducing strong  $\pi$ -donor substituent such as  $NH_2$  at para-position of vacant orbital, theoretical calculation and experimental results confirmed that phenyl cation will be triplet ground state in which one electron supplied from lone pair of  $NH_2$  to vacant  $sp^2$  orbital<sup>11-13</sup>. Additionally, in the vinyl cation case, which also has a vacant  $sp^2$  orbital, it was found from the theoretical calculation that by introducing  $\pi$ -donor (F, OMe,  $NH_2$ ,  $NMe_2$ ) at  $\beta$  position of cation, it will be triplet ground state<sup>14</sup>.

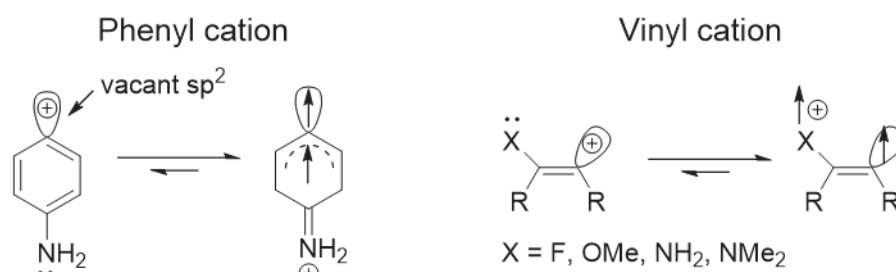


**Figure 2.** Triplet ground state carbocations bearing vacant  $sp^2$  orbital in its singlet state.

Furthermore, triplet carbocation which has *m*-xylylene-like electronic structure has been reported. *m*-xylylene is known as a non-Kekulé triplet ground state neutral molecule (Figure 3). Non-Kekulé molecules can be classified into 2 types; non-disjoint, in which singly occupied molecular orbital (SOMO) overlap spatially, and disjoint, in which SOMO do not overlap. Triplet of non-disjoint type non-Kekulé molecule can be stabilized by effective spin-spin

exchange interaction to make it triplet ground state.

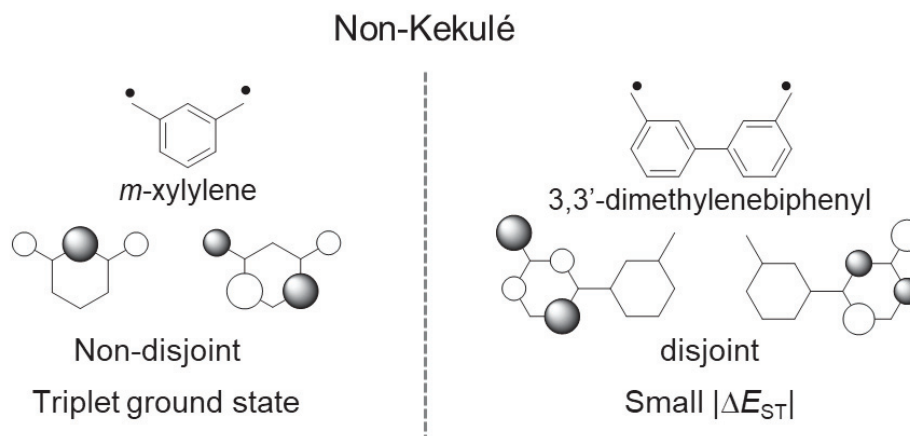


**Figure 3.** Non-Kekulé, non-disjoint and disjoint molecular structure and singly occupied MOs (SOMOs) of the triplet state.

Benzyl cations bearing strong  $\pi$ -donor substituent such as  $\text{NMe}_2$  at meta position of its cation were reported as one of the *m*-xylylene like triplet ground state carbocation<sup>15,16</sup> (Figure 4). Like benzyl cation, it was suggested from theoretical calculations that nitrenium ions<sup>17,18</sup> and oxenium ions<sup>15,19</sup> also have *m*-xylylene like triplet ground state ( $\pi$ ,  $\pi^*$  triplet) when introducing strong  $\pi$ -donor at meta position of its cation, and also, their triplets were directly observed by EPR measurements. Since the  $\pi$ -donor and  $\pi$ -acceptor (cation site) are located at a position where they are not directly conjugated, only the HOMO energy increases, the HOMO-LUMO gap becomes smaller, and the open-shell state becomes easier. Additionally, because SOMOs of these cations are non-disjoint type, exchange interaction can effectively work to make them triplet ground state. Based on this theory, it was also found by theoretical calculations that xanthene-based cations and (coumarin-4-yl)methyl cations bearing strong  $\pi$ -donor such as  $\text{NMe}_2$  at the position where not directly conjugate with cation have triplet ground state.<sup>20</sup>(Figure 4).

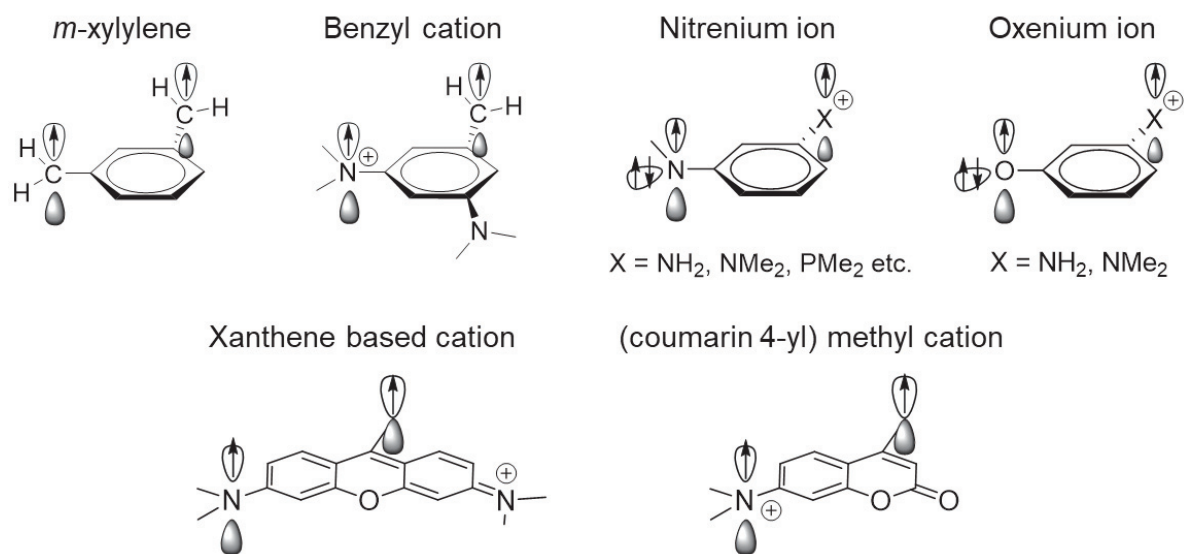


**Figure 4.** Triplet state of  $m$ -xylylene and triplet ground state ions.

#### **1-4. Purpose of this research**

The triplet carbocation, a novel electronic state carbocation known as an important reactive intermediate in the various field such as synthetic chemistry, biology and photo chemistry has been investigated both by theoretical and experimental approaches to develop new aspect of carbocation chemistry. In Chapter 2, triplet character of (7-diethylaminocoumarin -4-yl)methyl cation which is reactive intermediate of photo-induced leaving reaction, which is expected to be applicable to drug delivery system, was experimentally demonstrated. In Chapter 3, the novel triplet ground state indenyl cation was designed, and its substituent effects electronic ground state was investigated by theoretical calculations.



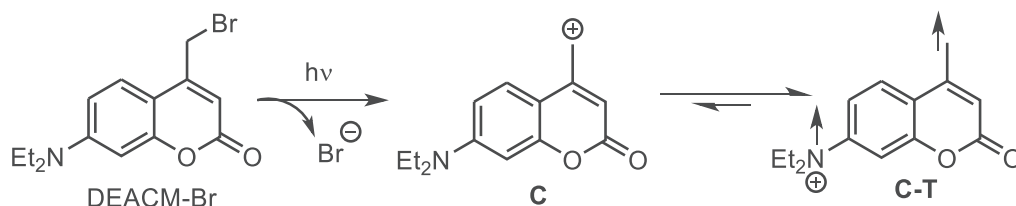


**Chapter 2.**

**Experimental Proof of Triplet Ground State  
Carbocation; (7-diethylaminocoumarin -4-yl)methyl  
cation**

## 2-1. Introduction

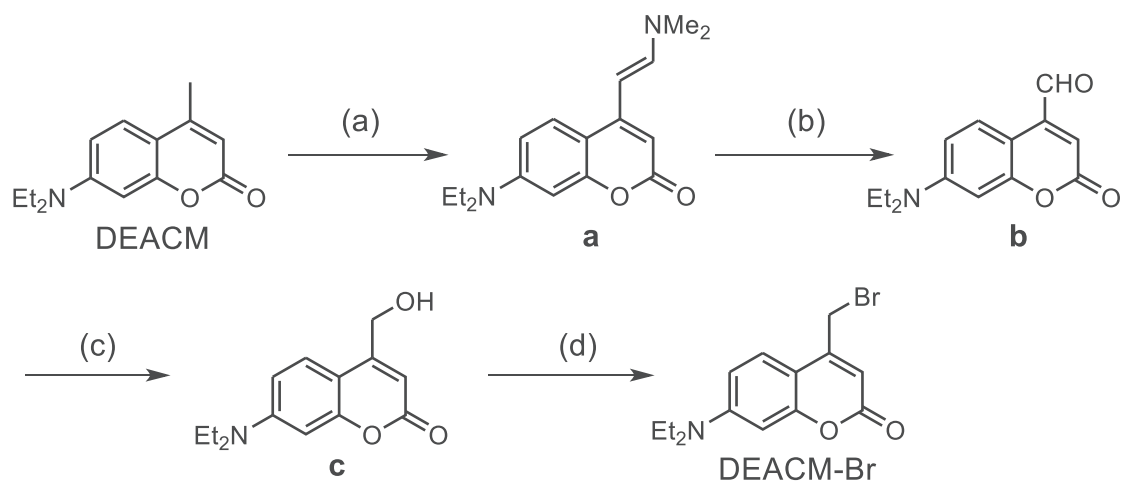
In this section, based on the suggestion in 2015 by DFT calculations that (7-diethylaminocoumarin -4-yl) methyl cation(C) has 9 kcal mol<sup>-1</sup> more stable triplet state(C-T), experimental demonstration and consideration of generation of C-T. (7-diethylaminocoumarin -4-yl)methyl coumarin(DEACM) is known as photolabile protecting group (PPG) which leaves target molecule introduced at methyl group at 4-position by photo-induced specific bond cleavage. In this study, generation of C-T was attempted by leaving Br<sup>-</sup> from DEACM-Br, which introduced bromide (Br) as leaving group, by photoirradiation (Scheme 1). DEACM-Br was synthesized, and its photoreaction mechanism was detailed investigated by low-temperature infrared (IR) spectroscopy, electron paramagnetic resonance (EPR) spectroscopy, and laser flash photolysis (LFP) measurements and product analysis to experimental demonstration of C-T and consideration of its generation mechanism.



**Scheme 1.** Generation of C-T from DEACM-Br by photoirradiation.

## 2-2. Synthesis and absorption spectrum measurement of DEACM-Br

DEACM-Br was synthesized by a known synthetic route<sup>21</sup> as shown in Scheme 2. Any purification was not conducted in the steps (a) and (b). The UV-visible absorption spectrum of DEACM-Br was measured in acetonitrile (ACN) (Figure 5) and the absorption band was mainly observed at 330 – 460 nm and below 290 nm. The 355 and 365 nm lights were used for excitation wavelength.



**Scheme 2.** Synthetic route of DEACM-Br; (a) DMF-DMA, DMF, 140°C, 14 h. (b) NaIO<sub>4</sub>, THF:H<sub>2</sub>O (1:1, v/v), RT, 2 h. (c) NaBH<sub>4</sub>, THF, RT, 2 h, 32%. (d) 1. NEt<sub>3</sub>, methanesulfonyl chloride, CH<sub>2</sub>Cl<sub>2</sub>, 0°C, 2 h, 2. LiBr, THF, RT, 2.5 h, 60%.

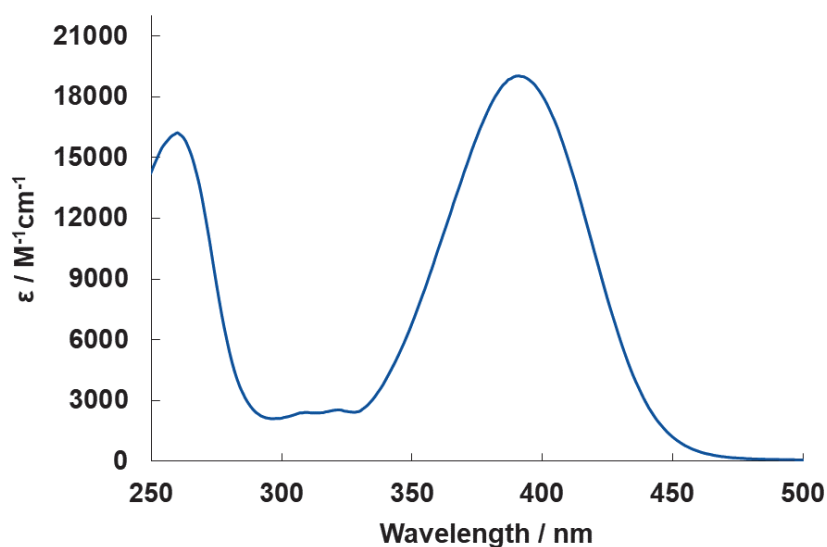


**Figure 5.** UV-vis absorption spectrum of DEACM-Br in acetonitrile.

### 2-3. Low-temperature IR and EPR measurements

To attempt direct observation of C-T, low-temperature IR and EPR measurements were conducted. IR measurement was conducted by irradiating 365 nm LED at 4 K to DEACM-Br:Ar = 1:1030 Ar matrix sample made at 20 K. After 23 h irradiation, the appearance of new signals was confirmed with decreasing of signals of DEACM-Br. (Figure 6). The new appeared signals were compared with simulation spectra of three predicted intermediate, radical

intermediate **D**, **C**, and **C-T**, obtained by DFT calculation (R/U/ B3LYP/6-31G(d,p)), which showed well matched with spectrum of **D**, and assigned to **D**.

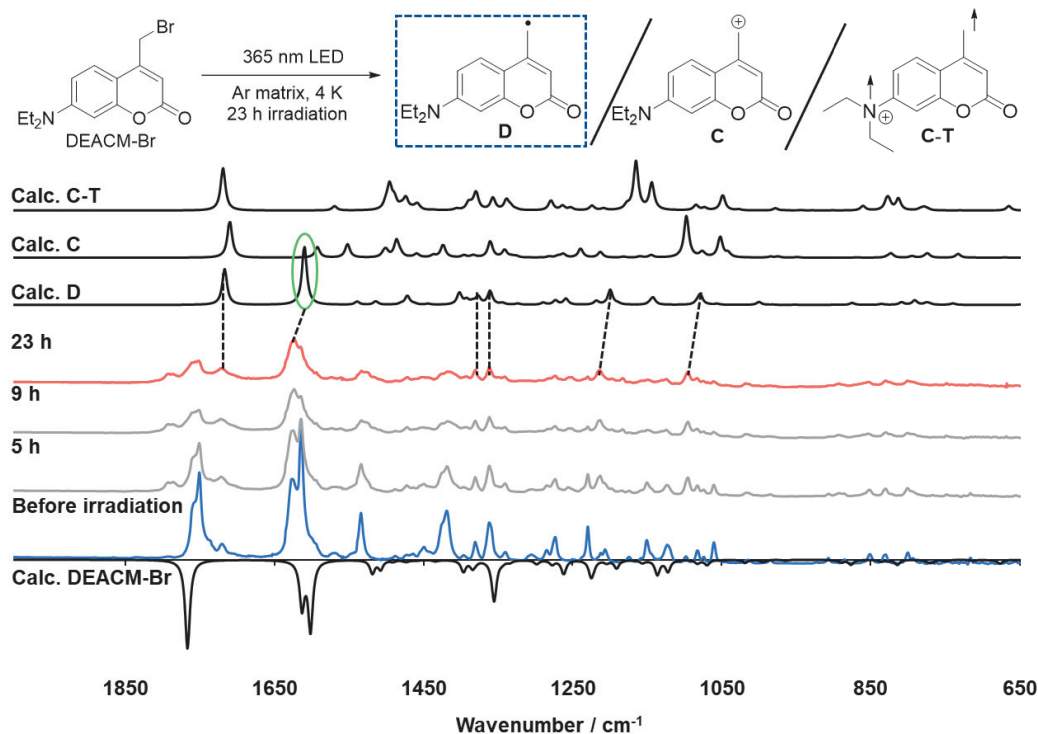


**Figure 6.** Low-temperature IR spectra in Ar matrix at 4 K irradiated 365 nm LED (before irradiation, after 5 h, 9 h and 23 h irradiation), and calculated (DFT R/UB3LYP/6-31G(d,p), scaled by 0.9613) spectra of DEACM-Br, **D**, **C** and **C-T** (The signals at 1627 and 1609  $\text{cm}^{-1}$ , which correspond to the symmetric and antisymmetric stretching vibrations of the aromatic ring, decrease with light irradiation, and the signal around 1630  $\text{cm}^{-1}$  increases. The signal at 1630  $\text{cm}^{-1}$  is considered to correspond to the signal at 1611  $\text{cm}^{-1}$ , which is one of the characteristic signal in computed IR spectrum of **D**. Several other signals that appeared with light irradiation were also in good agreement with the computed IR spectrum of **D**)

Low-temperature EPR measurements was conducted by irradiating 355 nm laser (10 mJ) at 10 K to 5 mM degassed DMSO solution of DEACM-Br. After 19 h irradiation, increasing of signal derived from radical species was observed (Figure 7). Because radical intermediate **D** was observed in low-temperature IR measurements, this signal is considered to derived from **D** (Scheme 4).

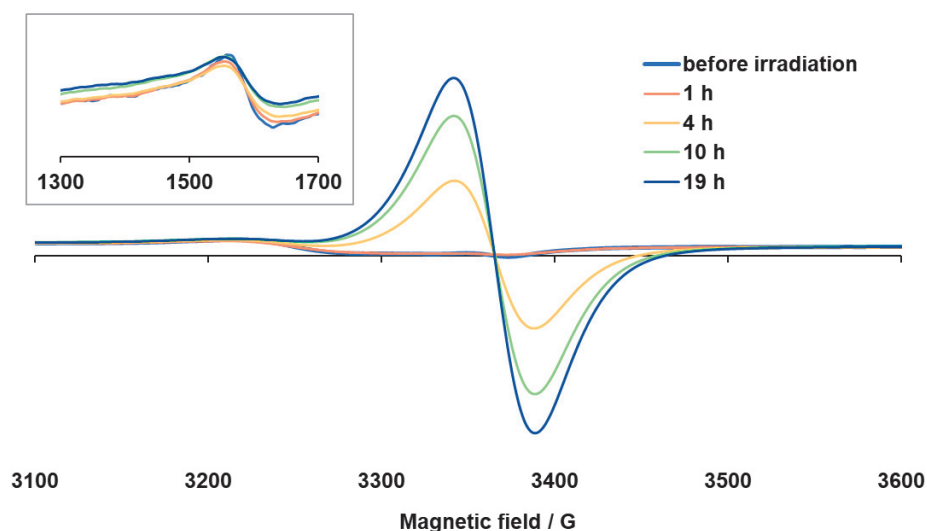
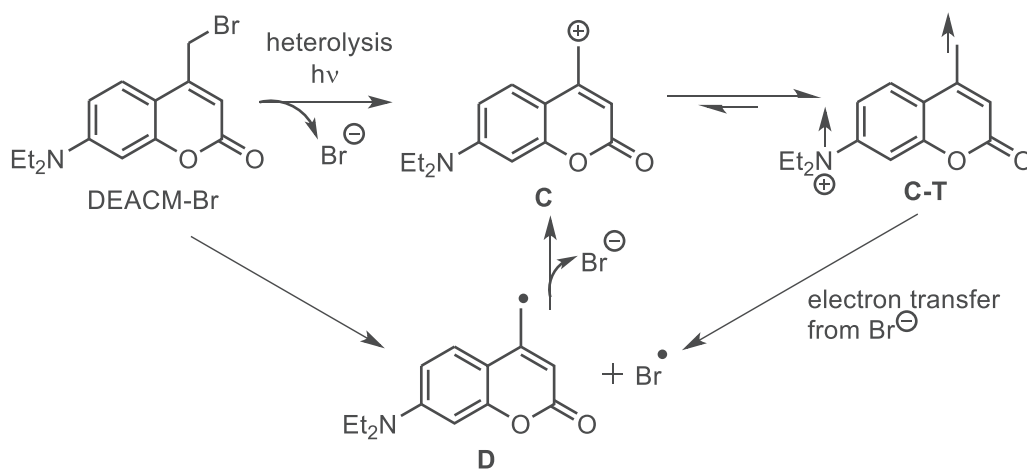


**Figure 7.** Low temperature EPR spectra in DMSO, at 10 K, irradiated 355 nm light (before irradiation, after 1 h, 4 h, 10 h and 19 h irradiation). Inset: half-field region. Parameters; Region: 1000-5000 G, Modulation amplitude: 19 G, Receiver gain: 60 dB, Power: 0.6325 mW, Conversion time: 2 ms, Number of points: 16384, Number of scans: 100



**Scheme 3.** Plausible mechanism of generation of **D**.

## 2-4. LFP measurements

To get further insight about the photoreaction mechanism of DEACM-Br, LFP measurements in acetonitrile (ACN) at room temperature (293 K) were conducted. 355 nm laser (Nd-YAG, 7-8 mJ/pulse, 4 ns pulse width) was used for pump light. ACN was used due to its polar nature, by which ionic species are stabilized. Firstly, the measurements were conducted for Ar-, Air-, and O<sub>2</sub>-saturated ACN solutions of DEACM-Br (0.1 mM, Abs = 0.80 at 355 nm). In the transient absorption (TA) spectrum of the Ar-saturated ACN solution, peaks corresponding to transient species were observed at 320 and 550 nm (Figure 8a). The decay at 320 nm was confirmed as multi-component decay (Figure 8b, blue). The rise process at 390 nm was observed as multi components kinetics (Figure 8b, green). The decay at 550 nm was fitted with a single exponential decay, and the rate constant was determined as  $k = 6.3 \times 10^4 \text{ s}^{-1}$  ( $\tau = 16 \text{ }\mu\text{s}$ ) (Figure 8b, orange). These all decay and rise process at 320, 390 and 550 nm were quenched in air- and O<sub>2</sub>-saturated ACN solutions (under air;  $k = 7.7 \times 10^5 \text{ s}^{-1}$ , under O<sub>2</sub>;  $k = 3.3 \times 10^6 \text{ s}^{-1}$ ) (Figure 8e). Additionally, because the TA spectrum peaks at 320 and 550 nm are well matched with computed UV-vis absorption spectrum of excited triplet state (T<sub>1</sub>) of DEACM-Br, that was identified as T-T absorption.

Because the TA peaks at 320 nm was well matched with calculated UV-vis absorption spectrum of **D**, it was considered to be derived from **D**. The observed range, approximately 360 – 440 nm, with a peak at 390 nm corresponds to the absorption region of DEACM-Br. Therefore, the multi components rise processes were considered to be the ground state recovery from T<sub>1</sub> to S<sub>0</sub> of DEACM-Br and recombination process following C-Br bond cleavage.

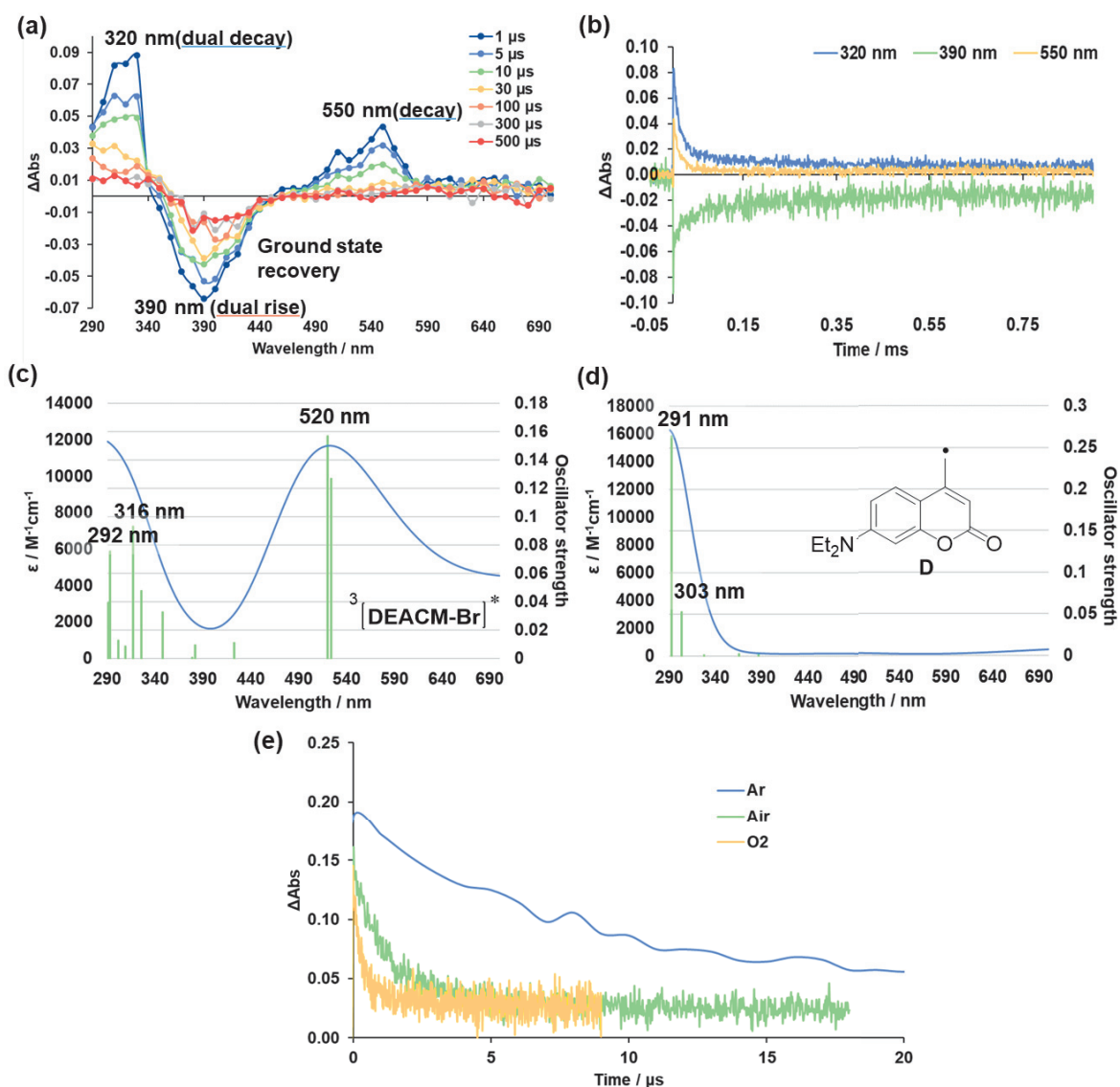


**Figure 8.** (a) TA absorption spectra in Ar-saturated ACN, (b) time profiles at 320, 390, and 550 nm in Ar-saturated ACN, (c) computed UV-vis absorption spectrum for  $T_1$  of DEACM-Br (UB3LYP/6-31G(d,p)), (d) computed UV-vis absorption spectrum of **D** (UB3LYP/6-31G(d,p)), (e) time profiles at 320 nm in Ar-, air-, and  $\text{O}_2$ -saturated ACN.

To further consideration of these identifications, LFP measurements of Ar-saturated ACN solutions of DEACM-Br (0.1 mM) in the presence of 0.05, 0.1, and 0.2 mM 2,2,6,6-tetramethylpiperidine-1-oxyl (TEMPO), which is a radical scavenger, were conducted. TA spectrum obtained in the presence of 0.2 mM TEMPO is shown in Figure 9a. The spectrum just after photoirradiation was similar to that in Figure 8a. The 320 nm decay was confirmed as multi-



component decay, and components observed in the measurements without TEMPO were completely quenched by TEMPO. Additionally, the single decay at 550 nm was also quenched by TEMPO;  $k = 1.3 \times 10^5 \text{ s}^{-1}$ ,  $1.8 \times 10^5 \text{ s}^{-1}$ , and  $3.6 \times 10^5 \text{ s}^{-1}$  in the presence of 0.05, 0.1, and 0.2 mM TEMPO, respectively. The multi-rise process at 390 nm were also quenched in the presence of TEMPO. The quenching of multi-components at 320 and 390 nm and the single decay at 550 nm by TEMPO can be explained by the deactivation of  $T_1$  of DEACM-Br was accelerated by TEMPO due to electron exchange process between  $T_1$  and TEMPO<sup>22</sup>, and also, radical **D** can be trapped by TEMPO. One of the components of multi-rise processes at 390 nm is the product generation process generated by trapping of **D** by TEMPO. This identification was supported by the UV-vis absorption spectrum after LFP measurements was blue-shifted to region where slower rise was observed (Figure 9c), and these generated products were identified by product analysis shown below.

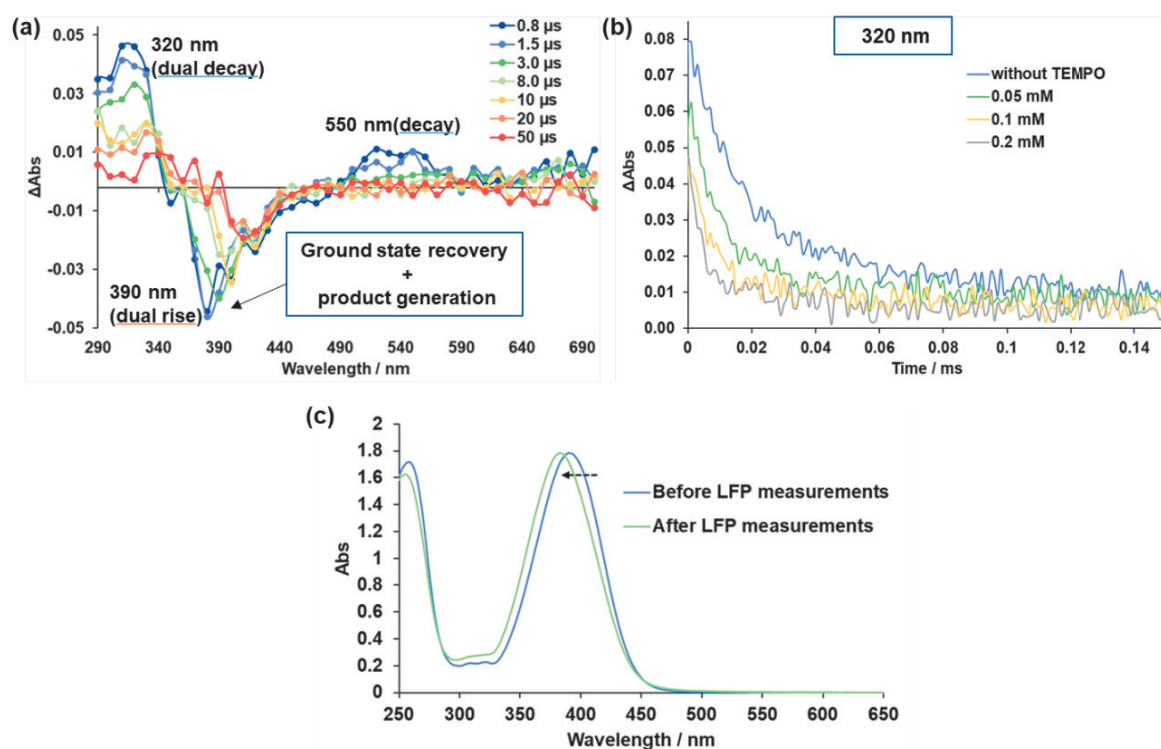


**Figure 9.** (a) TA absorption spectra in Ar-saturated ACN containing 0.2 mM TEMPO, (b) time profiles at 320 nm in Ar-saturated ACN containing 0, 0.05, 0.1, or 0.2 mM TEMPO, and (c) UV-vis absorption spectrum of before and after

LFP measurements of DEACM-Br (0.1 mM) Ar-saturated ACN containing 0.2 mM TEMPO.

## 2-5. Product analysis of DEACM-Br

For further understanding of photoreaction mechanism of DEACM-Br, product analysis was conducted for photoreaction of degassed (degassed by three freeze-pump-thaw cycles, and sealed NMR tube was used) and O<sub>2</sub>-saturated CD<sub>3</sub>CN solution of DEACM-Br (16 mM).

Photoreaction in degassed CD<sub>3</sub>CN was monitored by <sup>1</sup>H nuclear magnetic resonance (NMR) measurements. The spectrum after photo-irradiation was broadening and identification of the product was difficult (Figure 10). The photoreaction in O<sub>2</sub>-saturated CD<sub>3</sub>CN was also monitored by <sup>1</sup>H NMR. After irradiation, although the signal derived from proton of aldehyde product **b** and acetaldehyde **3** were observed, other signals in aromatic region were broadening and difficult to identify other products only from <sup>1</sup>H NMR. Therefore, to identify these products, photolysis of the O<sub>2</sub>-saturated ACN solution of DEACM-Br (26 mM, 200 mg) was performed on a larger scale under 365 nm LED irradiation. Trace amount of **c**, **1,2** and **b** was isolated by silica-gel column chromatography and identified by <sup>1</sup>H and <sup>13</sup>C NMR and ESI-MS measurements. Compound **b**, **c** and **1** were considered to generated by trapping of 4-methyl radical by O<sub>2</sub> (Scheme 4b). Because intermediate **D** and **C-T** both have 4-methyl radical, it was difficult to determine whether these products originate from **D** or **C-T**. The generation of compounds **1** and **2** indicate the generation of Br<sub>2</sub>, and it suggests homolytic bond cleavage of C-Br bond. The chemical yield of acetaldehyde **3** was determined as 8% from <sup>1</sup>H NMR. The formation of acetaldehyde in O<sub>2</sub>-saturated CD<sub>3</sub>CN can be explained by considering the reaction of singlet oxygen with the diethylamino group at the 7-position<sup>23,24</sup>(Scheme 4b). In the presence of 2-methyl-2-butene (400 mM) which is singlet oxygen quencher, acetaldehyde **3** was also detected in 10% yield, suggesting singlet oxygen reacts quickly with the amine moiety to give **3**. (Figure 20).

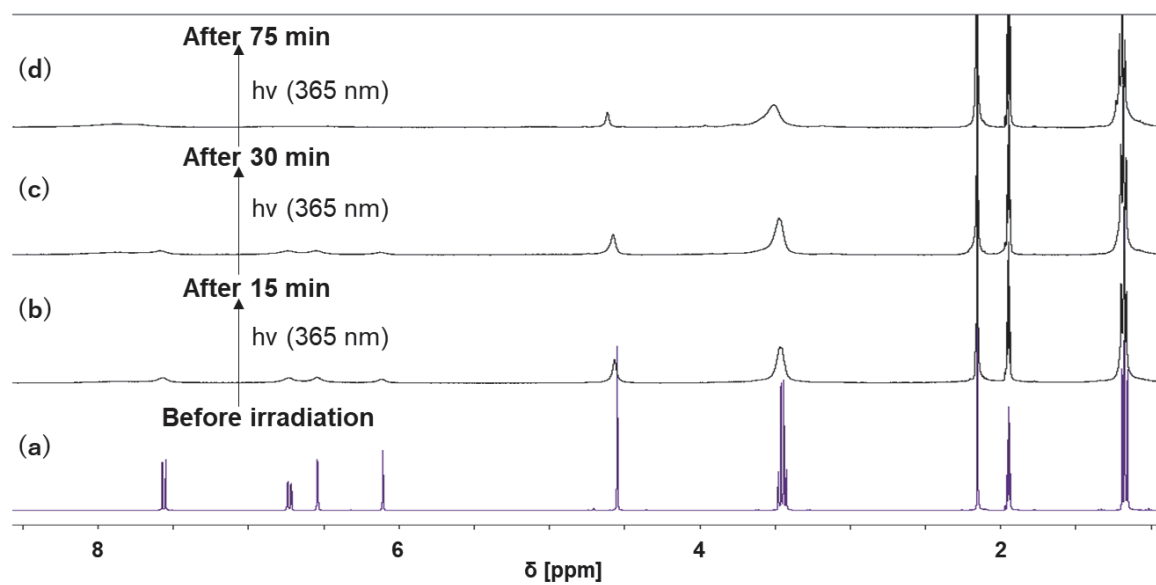
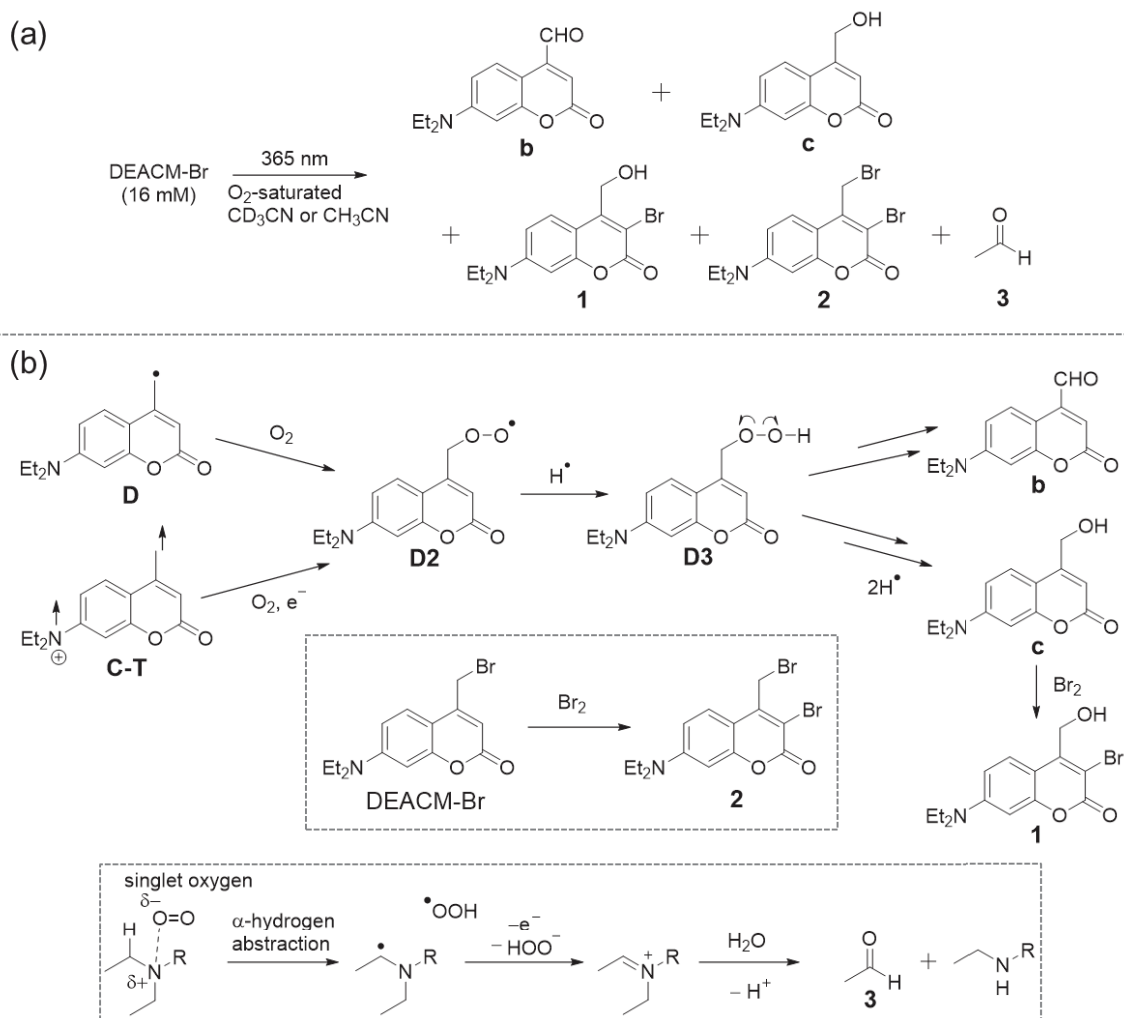


**Figure 10.** <sup>1</sup>H NMR spectra of the photolysis of DEACM-Br (16 mM) by 365 nm LED lamp in degassed CD<sub>3</sub>CN solution; (a) before irradiation, (b) after 15 min irradiation, (c) after 30 min irradiation, and (d) after 75 min irradiation.

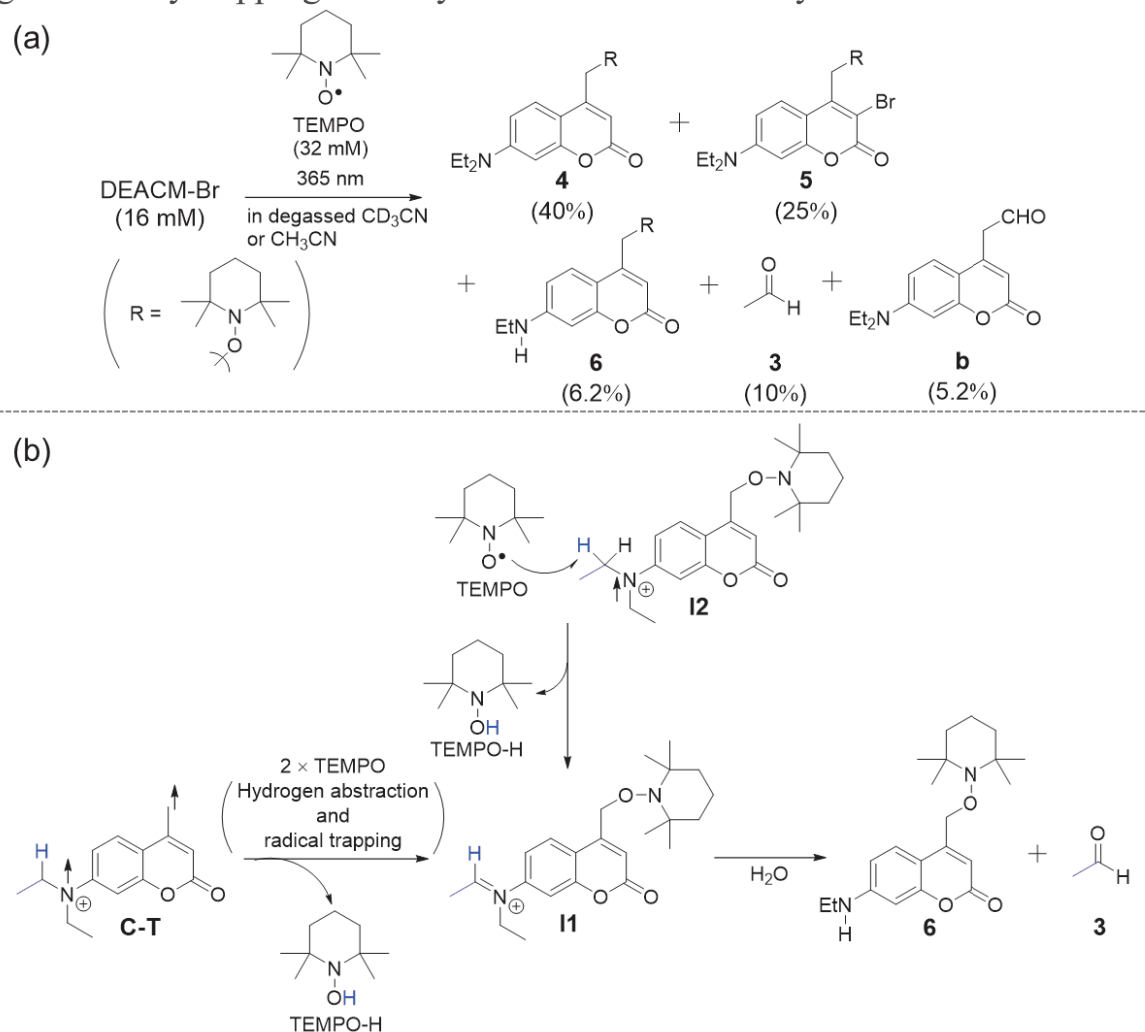


**Scheme 4.** (a) identified products of DEACM-Br in  $\text{O}_2$ -saturated  $\text{CD}_3\text{CN}$  (or ACN), and (b) generation mechanisms of identified products **b**, **c**, and **1-3**.

## 2-6. Product analysis of DEACM-Br in the presence of 2,2,6,6-tetramethylpiperidine-1-oxyl (TEMPO)

To get further insight, product analysis in the presence of TEMPO which is radical scavenger was conducted. The photolysis in degassed  $\text{CD}_3\text{CN}$  solution of DEACM-Br (16 mM) in the presence of 32 mM TEMPO in sealed NMR tube by 365 nm LED was monitored by  $^1\text{H}$  NMR (Figure 21), and confirmed the generation of compound **3** (6.2%) and **b** (5.2%). To identify other products, photolysis on a larger scale that in degassed ACN solution of DEACM-Br (16 mM, 80 mg) in the presence of 32 mM TEMPO by 365 nm LED was conducted. Compounds **4-6** were isolated by silica-gel column chromatography, and

identified by  $^1\text{H}$  and  $^{13}\text{C}$  NMR and ESI-MS measurements. Compounds **4**(40%) and **5**(25%) were main products, and they were considered to be generated by trapping 4-methyl radical of **D** or **C-T** by TEMPO.



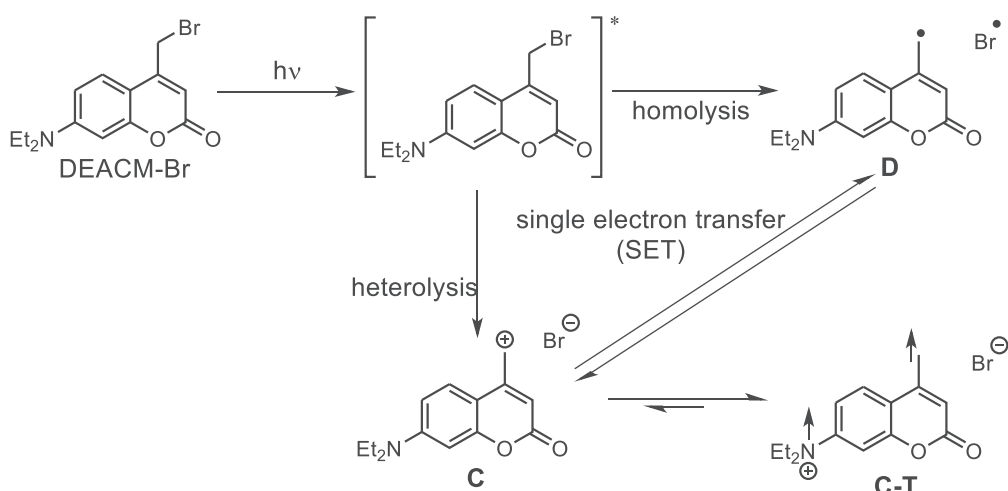
**Scheme 5.** (a) Identified photoreaction products of DEACM-Br in the presence of 32 mM TEMPO in degassed  $\text{CD}_3\text{CN}$ (ACN) (in the parentheses values under compound number are chemical yields), and (b) Generation mechanism of compound **6** and **3**.

Generation mechanism of compounds **6**(6.2%) and **3** should be noted (Scheme 5b). More specifically, hydrogen abstraction<sup>25–27</sup> of the  $\alpha$ -hydrogen atom of tertiary amine radical cation of the TEMPO-trapped adduct **I2** or **C-T** occurs to give the iminium ion intermediate **I1**, and this is followed by hydrolysis to produce acetaldehyde **3** and the secondary amine, **6**. To further confirm this reaction mechanism, the activation energy of  $\alpha$ -hydrogen

abstraction from radical cation diethylamino group at 7-position of **I2** or **C-T** by TEMPO were calculated at UB3LYP/6-31G(d,p) level of theory, and determined as 1.91 and 1.86 kcal/mol, respectively. Thus, this  $\alpha$ -hydrogen abstraction by TEMPO can easily occur at  $\sim 20^\circ\text{C}$  and generate compounds **6** and **3**. The formation of compounds **6** and **3** therefore is considered to be the first strong evidence of the generation of **C-T**.

## 2-7. Mechanism

The proposed photoreaction mechanism of DEACM-Br considered from experimental results is shown in Scheme 6. Generation mechanism of **C-T** can be explained by two pathways. One is generation by heterolytic bond cleavage of C-Br to generate **C** and **C-T**, and second is by single electron transfer from radical intermediate **D** to bromine radical to generate **C** and **C-T**. To consider the possibility of second path, firstly, the energy of radical pair [**D**, Br $\cdot$ ], ion pairs [**C**, Br $^-$ ] and [**C-T**, Br $^-$ ] were calculated at the (U or R)B3LYP/6-31G(d,p) level of theory with solvent effect of ACN by scrf method. [**C-T**, Br $^-$ ] was more stable, and [**D**, Br $\cdot$ ] was 16 kcal mol $^{-1}$  less stable than [**C-T**, Br $^-$ ]. [**C**, Br $^-$ ] was only 0.38 kcal mol $^{-1}$  unstable than [**D**, Br $\cdot$ ]. Furthermore, the redox potentials of **D** and Br $\cdot$  were calculated at the (U or R) M06-2x/6-31G(d,p) level<sup>28</sup> with solvent effect of ACN by scrf method determined as 1.73 and 1.40 V vs SCE, respectively. From these values,  $\Delta G$  of single electron transfer from **D** to Br $\cdot$  was calculated as  $\Delta G_{\text{SET}} = + 7.6$  kcal mol $^{-1}$ . From these results, [**C**, Br $^-$ ] can be generated from [**D**, Br $\cdot$ ] at room temperature, and generate more stable [**C-T**, Br $^-$ ].



**Scheme 6.** Photoreaction mechanism of DEACM-Br.

## 2-8. Conclusion

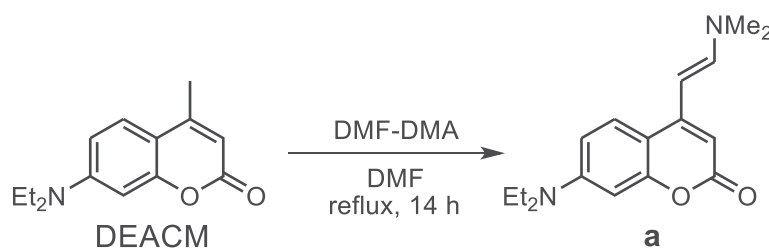
In this section, detail of photoreaction mechanism of DEACM-Br was investigated. In the product analysis of photolysis of DEACM-Br in the presence of TEMPO, first strong evidence of generation of **C-T** was found. Furthermore, the full picture of photoreaction mechanism of DEACM-Br was uncovered.

## 2-9. Experimental Section

### General Information

All commercially available reagents were purchased from TCI and Wako. NMR spectra were recorded on Bruker Ascend 400 ( $^1\text{H}$  NMR: 400 MHz,  $^{13}\text{C}$  NMR: 100 MHz) spectrometer at 298 K and referenced to residual solvent peak. Coupling constants ( $J$ ) are denoted in Hz and chemical shifts ( $\delta$ ) in ppm. The abbreviations s, d, t, q, dd and dq stand for the resonance multiplicities singlet, doublet, triplet, quartet, double of doublets and doublet of quartet, respectively. IR spectrum was recorded on a JASCO MCT-6000M. EPR spectra were recorded on a Bruker Bio Spin Elexsys E500. Mass spectrometric data were measured with Thermo Fisher Scientific LTQ Orbitrap XL. UV-vis spectra were recorded on a SHIMADZU UV-3600 Plus spectrometer. The spectra were collected at room temperature using a slit width of 1 nm with middle scan rate. The excitation source for sub-microsecond laser flash photolysis (LFP) was a tunable Nd:YAG minilite laser at 355 nm. The monitoring system consisted of a 150 W Xenon arc lamp as light source, a Unisoku MD200 monochromator detection and a photomultiplier.

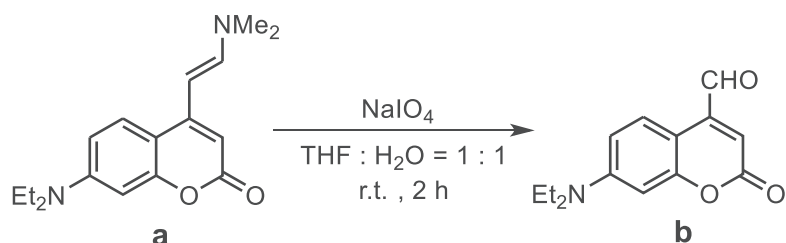
### Synthesis



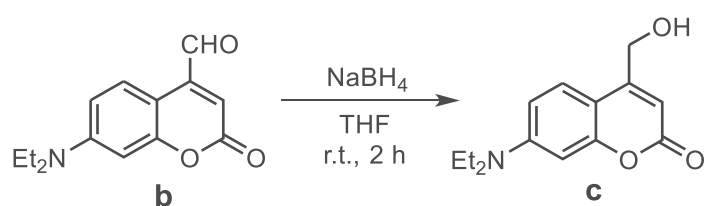
To a solution of DEACM (2.00 g, 8.64 mmol, 1.0 equiv.) in DMF (10 mL), DMF-DMA (2.3 mL, 17.3 mmol, 2.0 equiv.) was added. The reaction mixture was refluxed for 14 h under  $\text{N}_2$  atmosphere (at about 140 °C heated by an oil bath). Subsequently, conc.  $\text{NaHCO}_3$  and  $\text{CH}_2\text{Cl}_2$ . The reaction mixture was separated to aqueous layer and organic layer include compound **a** was extracted with  $\text{CH}_2\text{Cl}_2$ . Organic layer was dried with  $\text{Mg}_2\text{SO}_4$ , then filtered and the solvent was removed under reduced pressure. Any purification were not conducted.  $^1\text{H}$  NMR (400 MHz,  $\text{CDCl}_3$ ):  $\delta = 7.50$  (d,  $J = 8.0$  Hz, 1H, 5-H), 7.21 (d,  $J = 12$



Hz, 1H, CHCHN), 6.52 (dd,  $J = 8.0, 2.8$  Hz, 1H, 6-H), 6.46 (d,  $J = 1.2$  Hz, 1H, 8-H), 5.82 (s, 1H, 3-H), 5.20 (d,  $J = 14.8$  Hz, 1H, CHCHN), 3.38 (q,  $J = 4$  Hz, 4H, CH<sub>2</sub>CH<sub>3</sub>), 2.97 (s, 6H, N(CH<sub>3</sub>)<sub>2</sub>), 1.17 (t,  $J = 8$  Hz, 6H, CH<sub>2</sub>CH<sub>3</sub>).

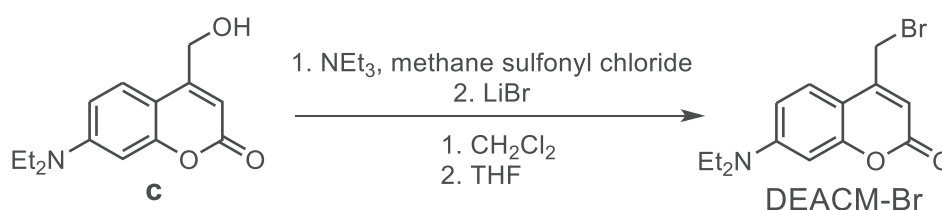


Residue of compound **a** was dissolved in THF/H<sub>2</sub>O (14 mL, 1:1) and NaIO<sub>4</sub> (5.54 g, 25.9 mmol, 3.0 equiv.) was added and stirred for 2 h at ambient temperature (~20 °C) under N<sub>2</sub> atmosphere. The precipitate was filtered off and washed with EtOAc. Half of solvent was removed under reduced pressure and added conc. NaHCO<sub>3</sub> solution. The products were extracted with CH<sub>2</sub>Cl<sub>2</sub> and organic layer was washed with H<sub>2</sub>O. Then, organic layer was dried with MgSO<sub>4</sub> and solvent was removed under reduced pressure. Any purification was not conducted. <sup>1</sup>H NMR (400 MHz, CDCl<sub>3</sub>) : $\delta$ = 10.02 (s, 1H, COH), 8.30 (d,  $J = 8.8$  Hz, 1H, 5-H), 6.62 (dd,  $J = 6, 2$  Hz, 1H, 6-H), 6.52 (d,  $J = 4$  Hz, 1H, 8-H), 6.45 (s, 1H, 3-H), 3.42 (q,  $J = 8$  Hz, 4H, CH<sub>2</sub>CH<sub>3</sub>), 1.21 (t,  $J = 8$  Hz, 6H, CH<sub>2</sub>CH<sub>3</sub>).



The residue of **b** was dissolved in THF (12 mL), cooled at 0 °C and added NaBH<sub>4</sub> (0.66 g, 17.3 mmol, 2.0 equiv.). Reaction mixture was stirred for 2 h at ambient temperature (~20 °C) under N<sub>2</sub> atmosphere. The reaction was quenched by adding NaHCO<sub>3</sub> solution and CH<sub>2</sub>Cl<sub>2</sub>. The organic layer was separated, and the aqueous layer was extracted with CH<sub>2</sub>Cl<sub>2</sub>. The organic layer was dried with MgSO<sub>4</sub> and solvent was removed under reduced pressure. **c** was purified by silica gel chromatography (EtOAc : Hexane = 1:1). **c** (680 mg, 31.8 % after 3

steps) was gained as yellow solid.  $^1\text{H}$  NMR (400 MHz, DMSO- $d_6$ ) : $\delta$ =7.43 (d,  $J$  = 8 Hz, 1H, 5-H), 6.66 (dd,  $J$  = 8, 4 Hz, 1H, 6-H), 6.52 (d,  $J$  = 4 Hz, 1H, 8-H), 6.06 (s, 1H, 3-H), 5.50 (t,  $J$  = 4 Hz, 1H, OH), 4.66 (dd,  $J$  = 4, 1.2 Hz, 2H,  $\text{CH}_2\text{OH}$ ), 3.42 (q,  $J$  = 5.6 Hz, 4H,  $\text{CH}_2\text{CH}_3$ ), 1.11 (t,  $J$  = 8 Hz, 6H,  $\text{CH}_2\text{CH}_3$ ).



**c** (100 mg, 0.404 mmol, 1.00 equiv.) was dissolved in  $\text{CH}_2\text{Cl}_2$  added  $\text{NEt}_3$  (0.116 mL, 0.808 mmol, 2.0 equiv.) and cooled at 0 °C. Methanesulfonyl chloride (0.0469 mL, 0.606 mmol, 1.5 equiv.) was added and stirred for 2 h at 0 °C under  $\text{N}_2$  atmosphere. The reaction was quenched with cooled conc.  $\text{NaHCO}_3$  solution and washed with cooled conc.  $\text{NaHCO}_3$  solution 2 times and dried with  $\text{MgSO}_4$ . Solvent was removed under reduced pressure and THF and LiBr (0.14 g, 1.616 mmol, 4.0 equiv.) were added to the residue. The reaction mixture was stirred for 2.5 h at ambient temperature ( $\sim 20$  °C). Solvent was removed under reduced pressure and the residue was solved in  $\text{CH}_2\text{Cl}_2$ . The solution was washed with brine and dried with  $\text{MgSO}_4$ . The solvent was removed under reduced pressure. DEACM-Br was purified by silica-gel column chromatography ( $\text{CH}_2\text{Cl}_2$  : EtOAc = 99:1) and yellow solid was obtained (75.1 mg, 60 %).  $^1\text{H}$  NMR (400 MHz,  $\text{CDCl}_3$ ) : $\delta$ =7.49 (d,  $J$  = 8 Hz, 1H, 5-H), 6.62 (dd,  $J$  = 4, 2.8 Hz, 1H, 6-H), 6.51 (d,  $J$  = 4 Hz, 1H, 8-H), 6.14 (s, 1H, 3-H), 4.40 (s, 2H,  $\text{CH}_2\text{Br}$ ), 3.42 (q,  $J$  = 8 Hz, 4H,  $\text{CH}_2\text{CH}_3$ ), 1.22 (t,  $J$  = 7 Hz, 6H,  $\text{CH}_2\text{CH}_3$ ).

## Supplementary Information of LFP measurements in Ar-, air-, and O<sub>2</sub>-saturated ACN

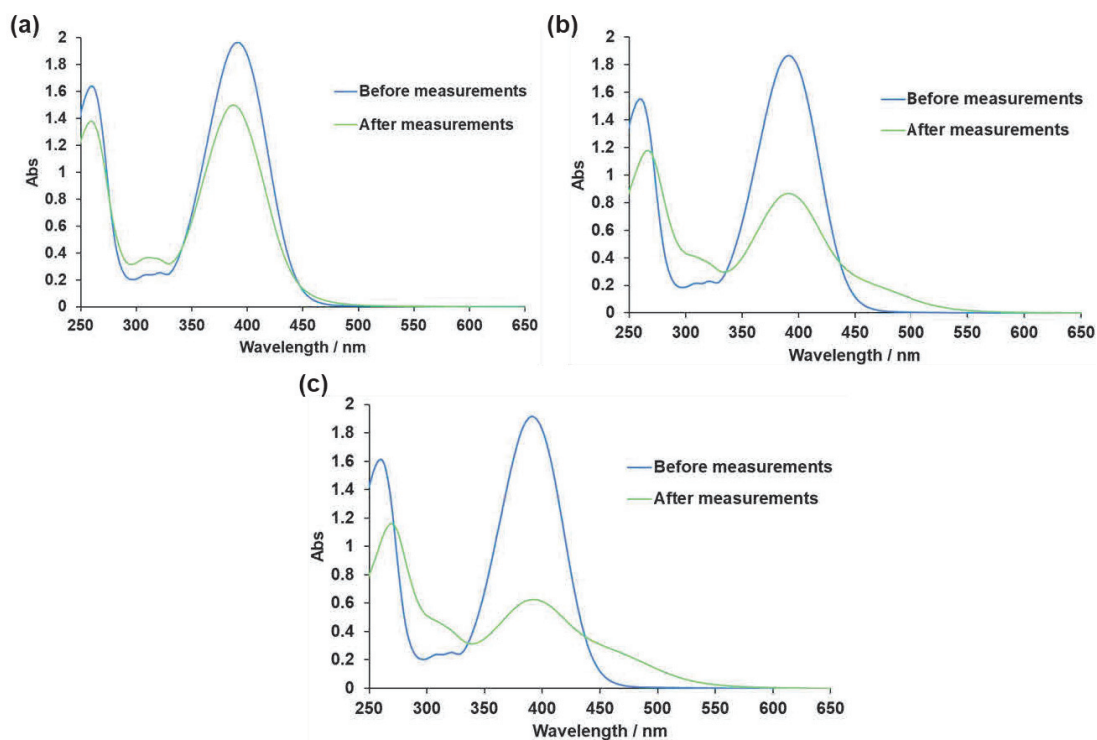


**Figure 11.** UV-vis absorption spectra of before and after LFP measurements; (a) in Ar-saturated ACN, (b) in air-saturated ACN, and (c) in O<sub>2</sub>-saturated ACN.

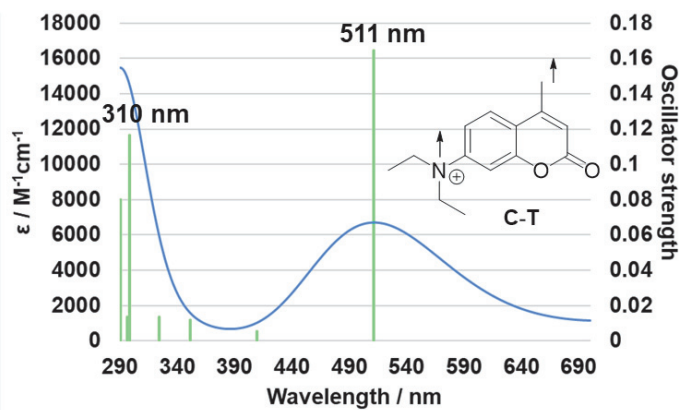


**Figure 12.** Computed UV-vis absorption spectrum of C-T (UB3LYP / 6-31G(d,p)).

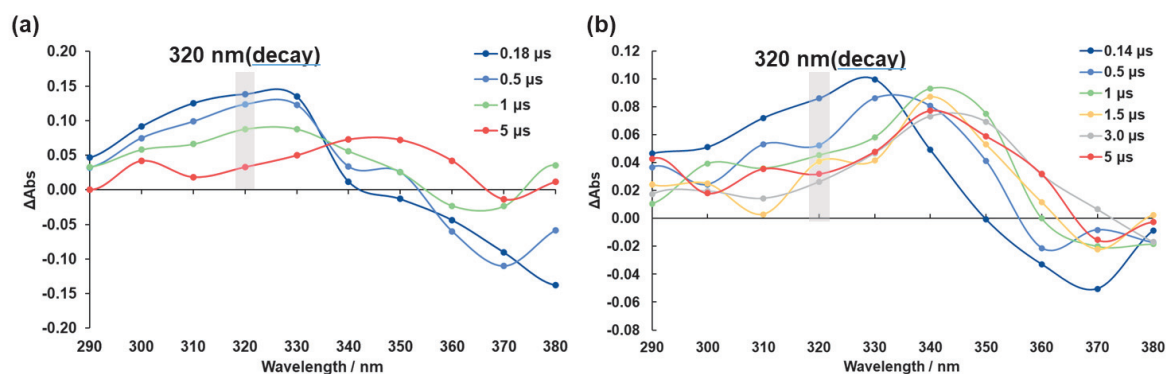


**Figure 13.** TA spectra (290-400 nm) of 0.20 mM solution measured in 5 mm cuvette; (a) in Air-saturated ACN (full time scale; 20  $\mu$ s), (b) in O<sub>2</sub>-saturated ACN (full time scale; 10  $\mu$ s).

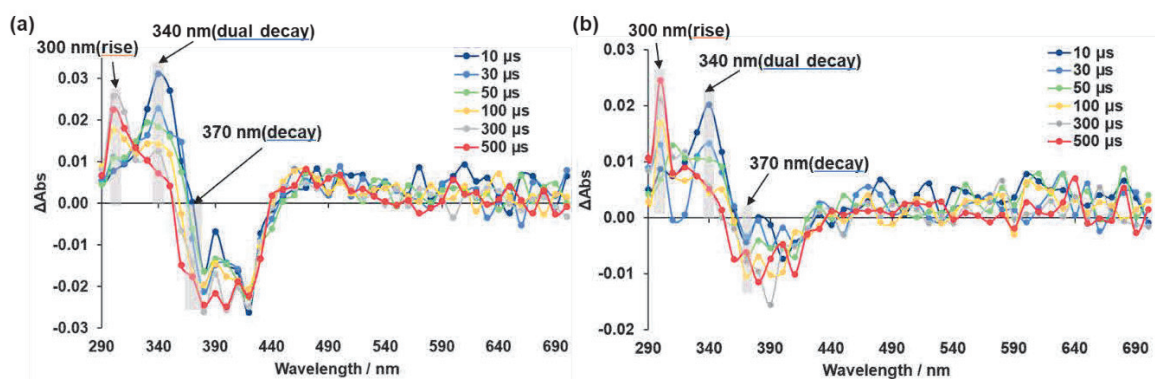


**Figure 14.** TA spectra (290-700 nm) of 0.10 mM solution measured in 10 mm cuvette; (a) in Air-saturated ACN (full time scale; 1 ms), (b) in O<sub>2</sub>-saturated ACN (full time scale; 1 ms).

**Table 1.** Time constants of 0.1 mM Air-saturated ACN solutions measured in 1 ms time scale. (blue : decay, red : rise)

	290 nm	300 nm	310 nm	320 nm	330 nm	340 nm	350 nm	360 nm
$\tau_1$	150 $\mu$ s	195 $\mu$ s	152 $\mu$ s	-	12.1 $\mu$ s	20.4 $\mu$ s	53.1 $\mu$ s	78.6 $\mu$ s
$\tau_2$					122 $\mu$ s	181 $\mu$ s	290 $\mu$ s	314 $\mu$ s
	370 nm	380 nm	390 nm	400 nm	410 nm			
$\tau_1$	157 $\mu$ s	119 $\mu$ s	199 $\mu$ s	183 $\mu$ s	160 $\mu$ s			

**Table 2.** Time constants of 0.1 mM O<sub>2</sub>-saturated ACN solutions measured in 1 ms time scale. (blue : decay, red : rise)

	290 nm	300 nm	310 nm	320 nm	330 nm	340 nm	350 nm	360 nm
$\tau_1$	155 $\mu$ s	144 $\mu$ s	163 $\mu$ s	-	27.3 $\mu$ s	13.7 $\mu$ s	182 $\mu$ s	
$\tau_2$					413 $\mu$ s	153 $\mu$ s		
	370 nm	380 nm	390 nm	400 nm	410 nm			
$\tau_1$	127 $\mu$ s	159 $\mu$ s	200 $\mu$ s	210 $\mu$ s	172 $\mu$ s			

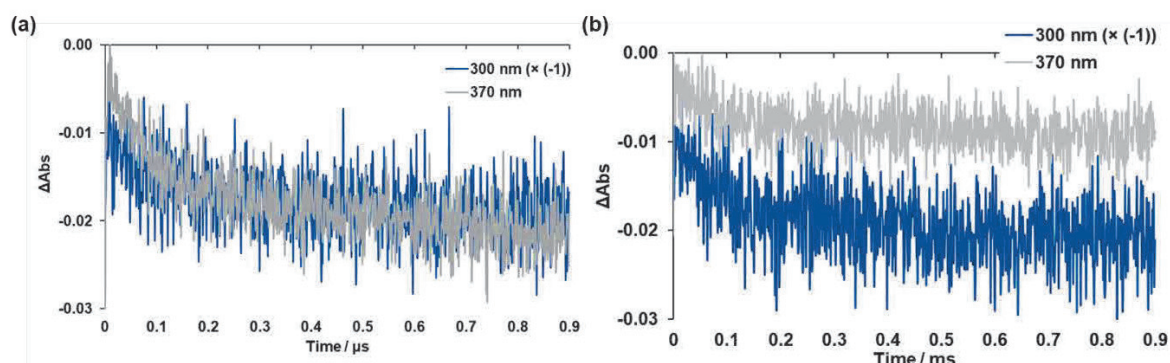


**Figure 15.** Time profiles at 300 nm ( $\times (-1)$ ) and 370 nm; (a) in Air-saturated ACN, (b) in O<sub>2</sub>-saturated ACN.

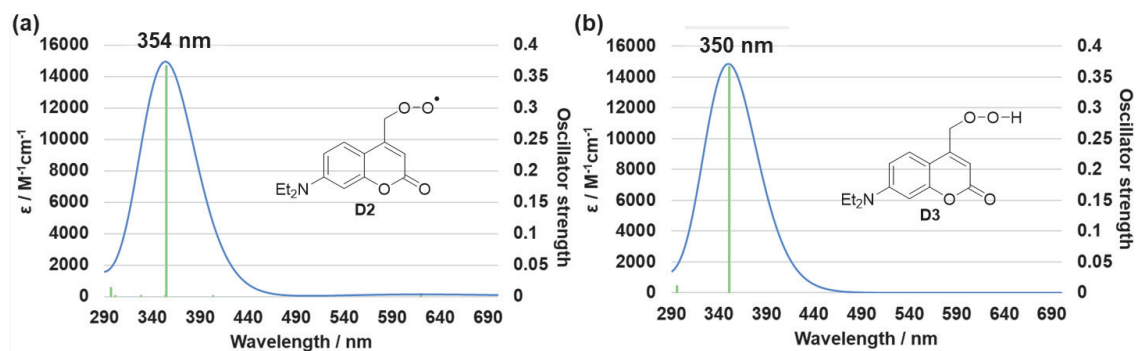


**Figure 16.** Computed UV-vis absorption spectra (u/rB3LYP/6-31G(d,p)); (a) D2, (b) D3.

## Supplementary Information of LFP measurements in Ar-saturated ACN presence of TEMPO

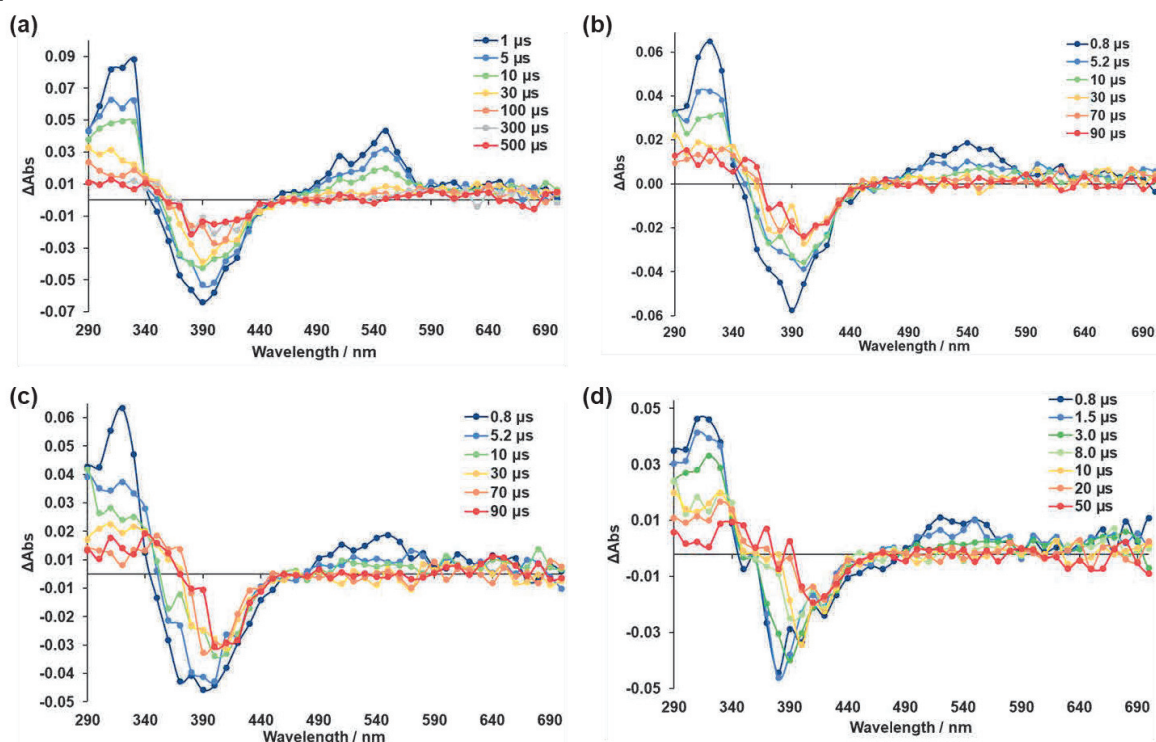


**Figure 17.** Transient absorption spectra of Ar-saturated ACN solutions; (a) without TEMPO, and in the presence of (b) 0.05 mM TEMPO, (c) 0.1 mM TEMPO, and (d) 0.2 mM TEMPO.

**Table 3.** Time constants of 0.05 mM TEMPO added Ar-saturated ACN solution. (blue : decay, red : rise)

	300 nm	310 nm	320 nm	330 nm	340 nm	350 nm	360 nm	370 nm
$\tau_1$	14.3 $\mu$ s (69 %)	9.48 $\mu$ s (82 %)	8.49 $\mu$ s (81 %)	11.1 $\mu$ s (72 %)	4.11 $\mu$ s	4.78 $\mu$ s	10.1 $\mu$ s (71 %)	9.77 $\mu$ s (52 %)
$\tau_2$	84.9 $\mu$ s (31 %)	86.7 $\mu$ s (18 %)	81.9 $\mu$ s (19 %)	76.0 $\mu$ s (28 %)	46.9 $\mu$ s	-	89.7 $\mu$ s (29 %)	71.4 $\mu$ s (48 %)
	380 nm	390 nm	400 nm	410 nm	420 nm	430 nm	490 nm	500 nm
$\tau_1$	11.9 $\mu$ s (56 %)	15.2 $\mu$ s (55 %)	11.9 $\mu$ s (80 %)	11.2 $\mu$ s (42 %)	5.32 $\mu$ s (57 %)	59 $\mu$ s	6.89 $\mu$ s	6.71 $\mu$ s
$\tau_2$	77.9 $\mu$ s (44 %)	92.3 $\mu$ s (45 %)	91.4 $\mu$ s (20 %)	74.3 $\mu$ s (58 %)	68.9 $\mu$ s (43 %)	-	-	-
	510 nm	520 nm	530 nm	540 nm	550 nm	560 nm	570 nm	
$\tau_1$	7.42 $\mu$ s	8.20 $\mu$ s	8.10 $\mu$ s	7.80 $\mu$ s	7.88 $\mu$ s	8.08 $\mu$ s	11.7 $\mu$ s	



300 - 330 nm : dual decay, 10  $\mu$ s + 80-90  $\mu$ s (peak : 320 nm (8.5  $\mu$ s + 90  $\mu$ s))

360 - 420 nm : dual rise, 10  $\mu$ s + 80-90  $\mu$ s (peak : 390 nm (15  $\mu$ s + 92.3  $\mu$ s))

490 - 570 nm : decay, 7-8  $\mu$ s (peak : 550 nm (7.9  $\mu$ s))

**Table 4.** Time constants of 0.1 mM TEMPO added Ar-saturated ACN solution.  
(blue : decay, red : rise)

	300 nm	310 nm	320 nm	330 nm	340 nm	350 nm	360 nm	370 nm
$\tau_1$	9.15 $\mu$ s (62 %)	4.04 $\mu$ s (61 %)	5.03 $\mu$ s (73 %)	3.26 $\mu$ s (46 %)	2.09 $\mu$ s	3.40 $\mu$ s (61 %)	5.69 $\mu$ s (43 %)	3.94 $\mu$ s (41 %)
$\tau_2$	36.6 $\mu$ s (38 %)	22.6 $\mu$ s (39 %)	28.0 $\mu$ s (27 %)	22.5 $\mu$ s (54 %)	12.8 $\mu$ s	34.9 $\mu$ s (39 %)	32.5 $\mu$ s (57 %)	30.9 $\mu$ s (59 %)
	380 nm	390 nm	400 nm	410 nm	420 nm	430 nm	490 nm	500 nm
$\tau_1$	10.6 $\mu$ s (70 %)	7.06 $\mu$ s (55 %)	5.35 $\mu$ s (46 %)	11.1 $\mu$ s	15.1 $\mu$ s	4.87 $\mu$ s	4.18 $\mu$ s	3.94 $\mu$ s
$\tau_2$	50.3 $\mu$ s (30 %)	31.9 $\mu$ s (45 %)	22.9 $\mu$ s (54 %)	-	-	-	-	-
	510 nm	520 nm	530 nm	540 nm	550 nm	560 nm	570 nm	
$\tau_1$	4.59 $\mu$ s	4.59 $\mu$ s	4.98 $\mu$ s	5.48 $\mu$ s	5.49 $\mu$ s	6.18 $\mu$ s	5.60 $\mu$ s	

300 - 330 nm : dual decay, 5  $\mu$ s + 20-30  $\mu$ s (peak : 320 nm (5.0  $\mu$ s + 28  $\mu$ s))

360 - 420 nm : dual rise, 5  $\mu$ s + 30  $\mu$ s (peak : 390 nm (7.1  $\mu$ s + 32  $\mu$ s))

490 - 570 nm : decay, 5  $\mu$ s (peak : 550 nm (5.5  $\mu$ s))

**Table 5.** Time constants of 0.2 mM TEMPO added Ar-saturated ACN solution.  
(blue : decay, red : rise)

	300 nm	310 nm	320 nm	330 nm	340 nm	350 nm	360 nm	370 nm
$\tau_1$	10.1 $\mu$ s	1.52 $\mu$ s (44 %)	3.03 $\mu$ s (67 %)	3.80 $\mu$ s (53 %)	717 ns	11.2 $\mu$ s	10.2 $\mu$ s	9.90 $\mu$ s
$\tau_2$	-	10.1 $\mu$ s (56 %)	13.7 $\mu$ s (33 %)	14.8 $\mu$ s (47 %)	7.28 $\mu$ s	-	-	-
	380 nm	390 nm	400 nm	410 nm	420 nm	430 nm	490 nm	500 nm
$\tau_1$	10.3 $\mu$ s	10.0 $\mu$ s	10.1 $\mu$ s	10.9 $\mu$ s	219 ns	-	-	2.17 $\mu$ s
$\tau_2$	-	-	-	-	-	-	-	-
	510 nm	520 nm	530 nm	540 nm	550 nm	560 nm	570 nm	

$\tau_1$     3.14  $\mu\text{s}$     1.79  $\mu\text{s}$     2.41  $\mu\text{s}$     2.40  $\mu\text{s}$     2.76  $\mu\text{s}$     3.26  $\mu\text{s}$     4.76  $\mu\text{s}$

300 - 330 nm : dual decay, 2  $\mu\text{s}$  + 10  $\mu\text{s}$  (peak : 320 nm (3.0  $\mu\text{s}$  + 14  $\mu\text{s}$ ))

360 - 420 nm : dual rise, 10  $\mu\text{s}$  (peak : 390 nm (10  $\mu\text{s}$ )) fast rise could not be fitted.

500 - 570 nm : decay, 2  $\mu\text{s}$  (peak : 550 nm (2.8  $\mu\text{s}$ ))

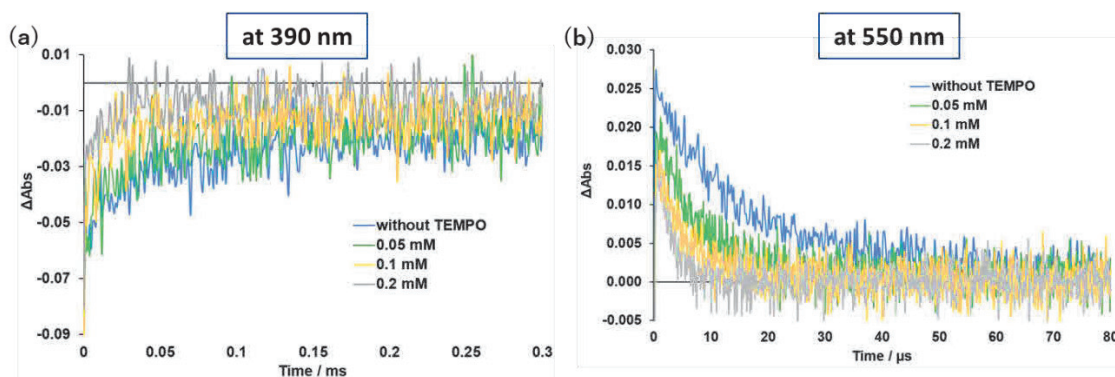


**Figure 18.** Time profiles of without TEMPO and added 0.05 mM, 0.1 mM, or 0.2 mM TEMPO; (a) at 390 nm, (b) at 550 nm.

### Supplementary Information of product analysis of DEACM-Br

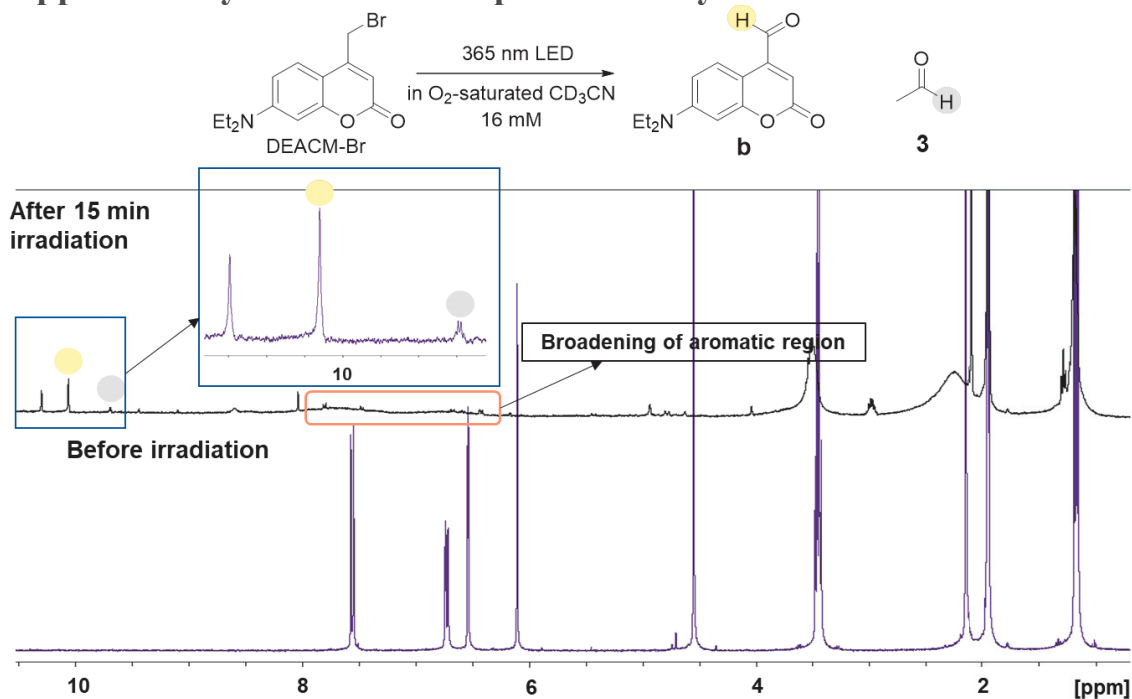


**Figure 19.**  $^1\text{H}$  NMR analysis of photolysis of DEACM-Br (16 mM) irradiated by 365 nm LED in  $\text{O}_2$ -saturated  $\text{CD}_3\text{CN}$ .



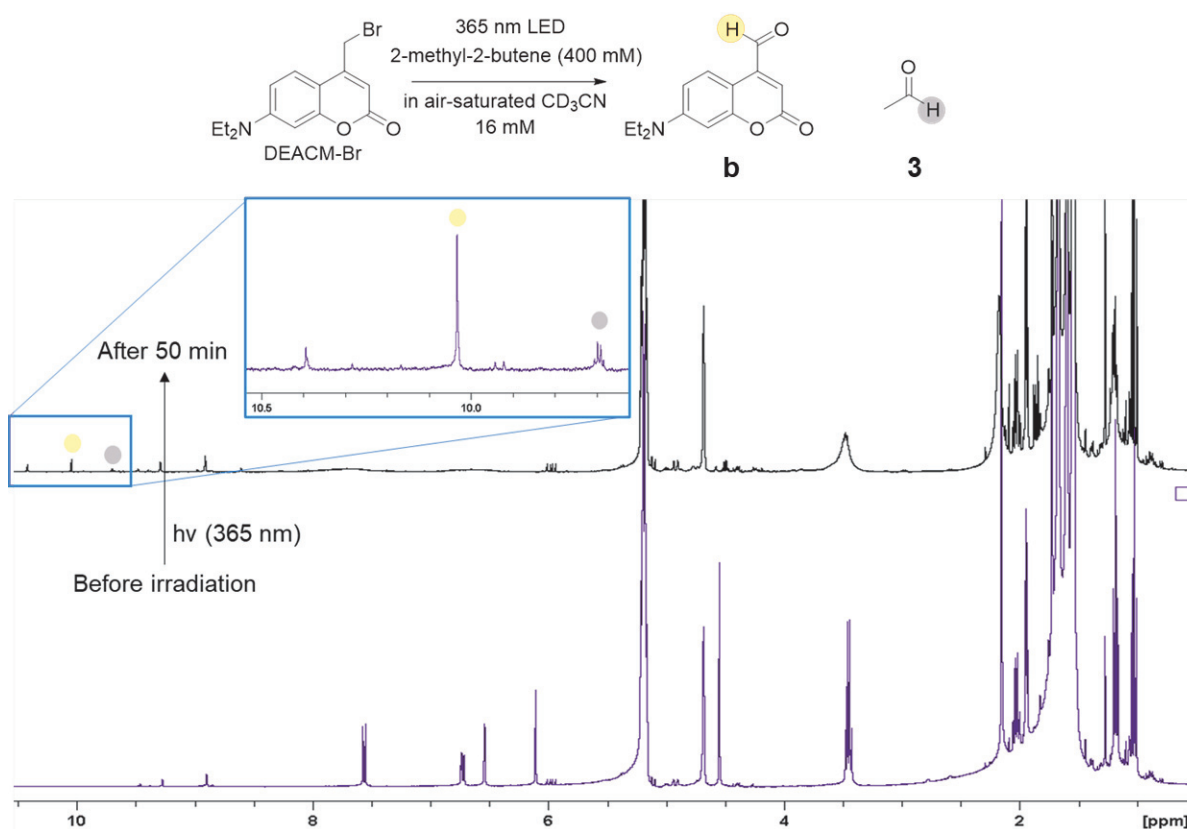


**Figure 20.**  $^1\text{H}$  NMR analysis of photolysis of DEACM-Br (16 mM) in the presence of 400 mM 2-methyl-2-butene irradiated by 365 nm LED in  $\text{O}_2$ -saturated  $\text{CD}_3\text{CN}$ .

Characterization of Compound **1** and **2** by  $^1\text{H}$ ,  $^{13}\text{C}$  NMR and ESI-HRMS measurements

[Compound **1**]

$^1\text{H}$  NMR (400 MHz,  $\text{CD}_3\text{CN}$ ) :  $\delta$ =7.72 (d,  $J$  = 9.2 Hz, 1H), 6.73 (dd,  $J$  = 9.2, 2.6 Hz, 1H), 6.54 (d,  $J$  = 2.6 Hz, 1H), 4.86 (d,  $J$  = 6.0 Hz, 2H), 3.51 (t,  $J$  = 6.1 Hz, 1H), 3.44 (q,  $J$  = 7.1 Hz, 4H), 1.17 (t,  $J$  = 7.1 Hz, 6H).  $^{13}\text{C}$  NMR (100 MHz,  $\text{CD}_3\text{CN}$ ) :  $\delta$ =206.41, 155.21, 151.80, 127.22, 109.21, 107.53, 104.71, 96.72, 60.88, 44.35, 29.86, 11.71. HRMS (p-ESI, MeOH sol)  $m/z$  : Calcd for  $\text{C}_{14}\text{H}_{17}\text{O}_3\text{NBr}$  [ $\text{M} + \text{H}$ ] $^+$ , 326.03863, found 326.03891.

[Compound **2**]

$^1\text{H}$  NMR (400 MHz,  $\text{CD}_3\text{CN}$ ) :  $\delta$ =7.56 (d,  $J$  = 9.2 Hz, 1H), 6.77 (dd,  $J$  = 9.2, 2.6 Hz, 1H), 6.56 (d,  $J$  = 2.6 Hz, 1H), 4.73 (s, 2H), 3.45 (q,  $J$  = 7.1 Hz, 4H), 1.17 (t,  $J$  = 7.1 Hz, 6H).  $^{13}\text{C}$  NMR (100 MHz,  $\text{CD}_3\text{CN}$ ) :  $\delta$ =158.64, 156.20, 152.29, 127.10, 110.49, 107.09, 106.44, 98.05, 45.45, 28.38, 12.71. HRMS (p-ESI,

MeOH sol)  $m/z$  : Calcd for  $C_{14}H_{15}O_2NBr^{81}BrNa [M + Na]^+$ , 411.93413, found 411.93430.

### Supplementary Information of product analysis of DEACM-Br in the presence of TEMPO

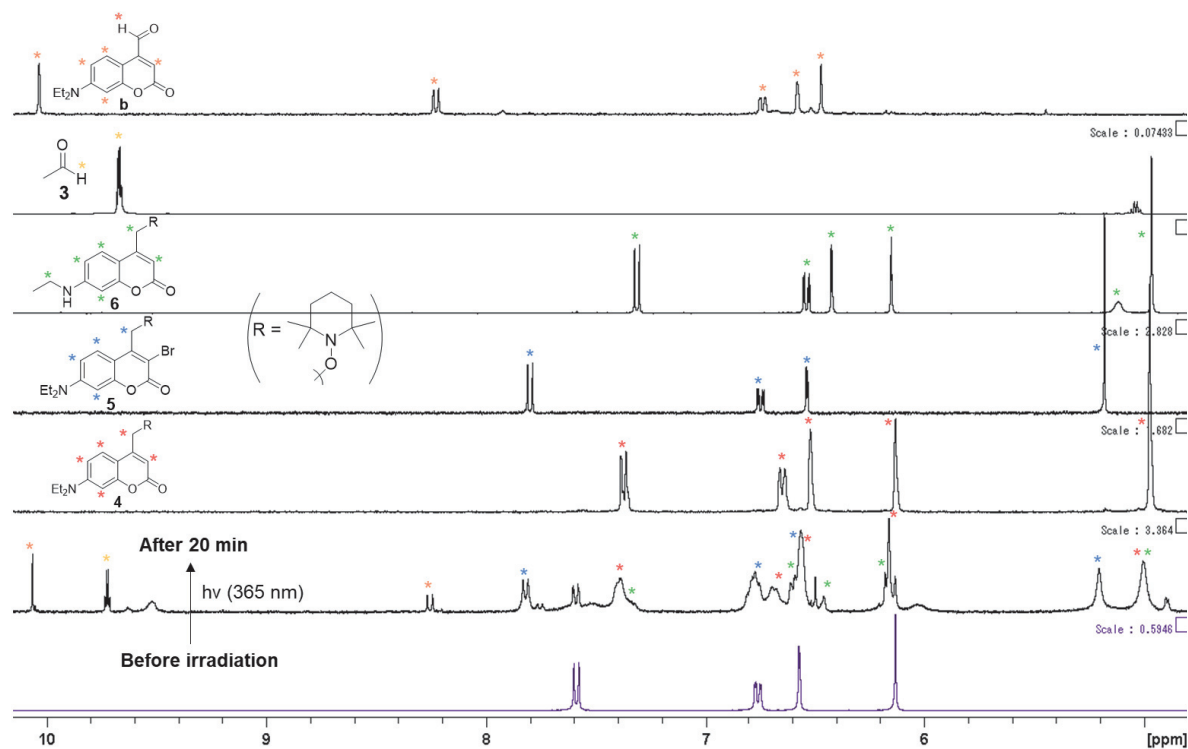


**Figure 21.**  $^1H$  NMR analysis of photolysis of DEACM-Br (16 mM) in the presence of 32 mM TEMPO irradiated by 365 nm LED in degassed  $CD_3CN$  (4.8 – 10.2 ppm).

### Characterization of Compound 4, 5 and 6 by $^1H$ , $^{13}C$ NMR and ESI-HRMS measurements

[Compound 4]

$^1H$  NMR (400 MHz,  $CD_3CN$ ) :  $\delta$ =7.37 (d,  $J$  = 9.0 Hz, 1H), 6.64 (dd,  $J$  = 9.0, 2.6 Hz, 1H), 6.52 (d,  $J$  = 2.6 Hz, 1H), 6.13 (t,  $J$  = 1.4 Hz, 1H), 4.97 (d,  $J$  = 1.4 Hz, 2H), 3.43 (q,  $J$  = 7.0 Hz, 6H), 1.66-1.58 (m, 1H), 1.55-1.42 (m, 4H), 1.38-1.92 (m, 1H), 1.21-1.13 (m, 18H).  $^{13}C$  NMR (100 MHz,  $CD_3CN$ ) :  $\delta$ =162.56, 157.27, 153.62, 151.72, 126.26, 109.55, 106.08, 98.18, 75.49, 60.86, 45.28, 40.52, 33.35, 20.66, 17.78, 12.74. HRMS (p-ESI, MeOH sol)  $m/z$  : Calcd for  $C_{23}H_{34}O_3N_2Na [M + Na]^+$ , 409.24616, found 409.24622.

[Compound 5]

<sup>1</sup>H NMR (400 MHz, CD<sub>3</sub>CN) : $\delta$ =7.83 (d,  $J$  = 9.2 Hz, 1H), 6.77 (dd,  $J$  = 9.2, 2.7 Hz, 1H), 6.56 (d,  $J$  = 2.6 Hz, 1H), 5.21 (s, 1H), 3.48 (q,  $J$  = 7.1 Hz, 4H), 1.67-1.57 (m, 1H), 1.56-1.48 (m, 4H), 1.47-1.41 (m, 1H), 1.26 (s, 6H), 1.20 (t,  $J$  = 7.1 Hz, 6H), 1.11 (s, 6H). <sup>13</sup>C NMR (100 MHz, CD<sub>3</sub>CN) : $\delta$ =157.92, 155.05, 150.87, 150.24, 128.22, 109.03, 107.76, 104.50, 96.58, 77.09, 59.74, 44.35, 39.53, 32.77, 19.52, 16.77, 11.73. HRMS (p-ESI, MeOH sol)  $m/z$  : Calcd for C<sub>23</sub>H<sub>34</sub>O<sub>3</sub>N<sub>2</sub>Br [M + H]<sup>+</sup>, 465.17473, found 465.17429.

[Compound 6]

<sup>1</sup>H NMR (400 MHz, CD<sub>3</sub>CN) : $\delta$ =7.31 (d,  $J$  = 8.8 Hz, 1H), 6.53 (dd,  $J$  = 8.8, 2.3 Hz, 1H), 6.42 (d,  $J$  = 2.3 Hz, 1H), 6.15 (t,  $J$  = 1.4 Hz, 1H), 5.12 (s, 1H), 4.97 (d,  $J$  = 1.4 Hz, 2H), 3.17 (dq,  $J$  = 7.2 Hz, 2H), 1.70-1.57 (m, 1H), 1.56-1.40 (m, 2H), 1.39-1.30 (m, 1H), 1.21 (t,  $J$  = 7.2 Hz, 3H), 1.19 (s, 6H), 1.18 (s, 6H). <sup>13</sup>C NMR (100 MHz, CD<sub>3</sub>CN) : $\delta$ =161.42, 156.27, 152.75, 152.34, 125.06, 110.21, 106.93, 105.24, 96.96, 74.42, 59.84, 39.49, 37.52, 32.31, 19.64, 16.75, 13.36. HRMS (p-ESI, MeOH sol)  $m/z$  : Calcd for C<sub>21</sub>H<sub>31</sub>O<sub>3</sub>N<sub>2</sub> [M + H]<sup>+</sup>, 359.23292, found 359.23282.

**Determination of photoproduct chemical yield (compound b and 3-6)**

Triphenylmethane (TPM) was used as internal standard.

1. 64.3 mM CD<sub>3</sub>CN solution of TPM was prepared in 1 mL volumetric flask.
2. 64.3 mM TPM solution was added 0.1 mL to photoreaction solution and then, <sup>1</sup>H NMR was measured.
3. From <sup>1</sup>H NMR spectrum of the mixture of TPM and photoreaction solution, we calculated the integral value of DEACM-Br, compound **b**, **3-6** based on that of TPM (1H), and then the amount of the unreacted DEACM-Br (mmol) and the generated compounds were determined from eq. (1) and (3) respectively. The conversion yield (%) of DEACM-Br and chemical yield of photoproducts were calculated from eq. (2) and (4) respectively.

(The amount of unreacted DEACM-Br )

$$= (\text{The amount of TPM (mmol)}) \times (\text{The integral value of DEACM-Br after photoreaction (1H)}) \dots (1)$$

(The conversion yield (%) )

$$= \frac{(\text{The amount of DEACM-Br before photoreaction} - \text{The amount of unreacted DEACM-Br (mmol)})}{(\text{The amount of DEACM-Br before photoreaction (mmol)})} \times 100 \dots (2)$$

(The amount of photoproduct)

$$= (\text{The amount of the unreacted DEACM-Br (mmol)}) \times (\text{The integral value of photoproduct (1H)}) \dots (3)$$

(The chemical yield of photoproduct (%) )

$$= \frac{(\text{The amount of photoproduct (mmol)})}{(\text{The amount of consumed DEACM-Br by photoreaction (mmol)})} \times 100 \dots (4)$$

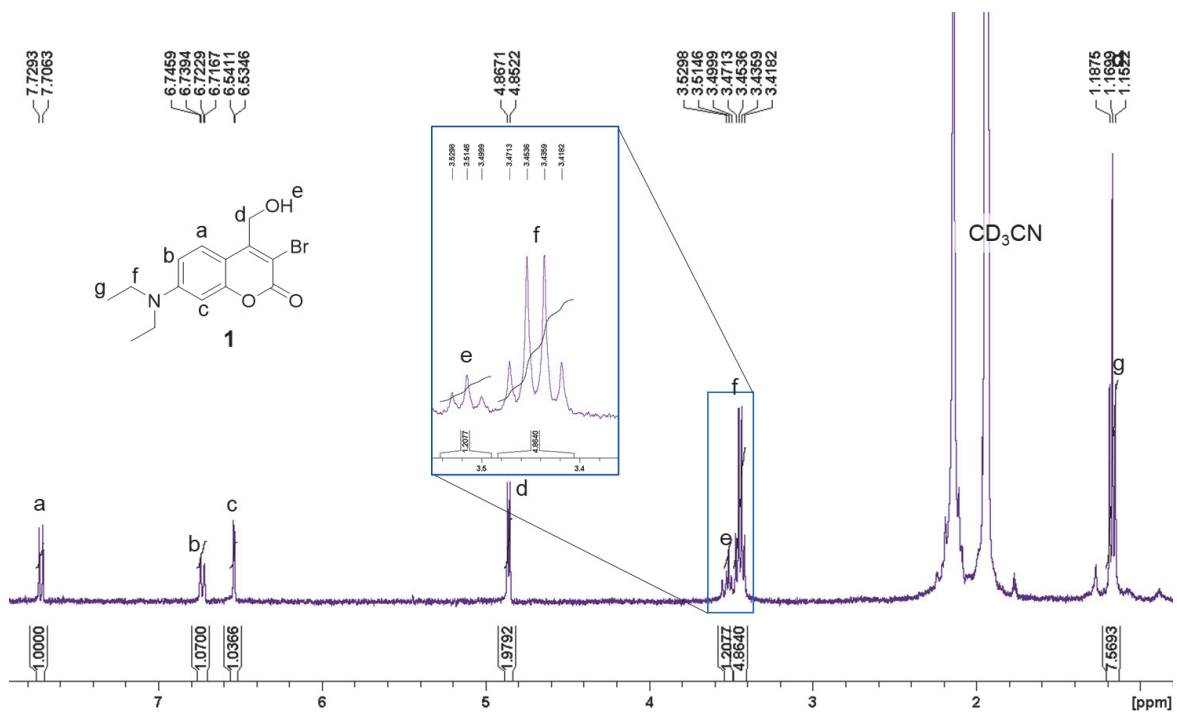


Figure 22. <sup>1</sup>H NMR of compound 1 in CD<sub>3</sub>CN.

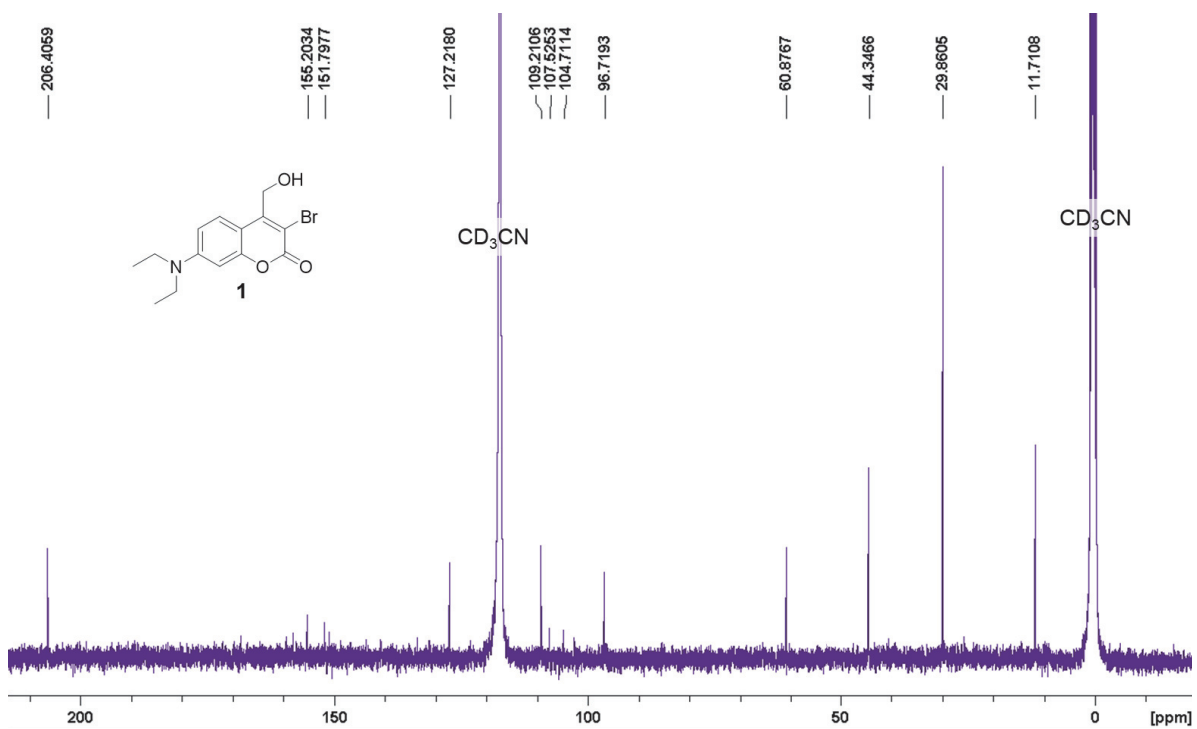


Figure 23. <sup>13</sup>C NMR of compound 1 in CD<sub>3</sub>CN.

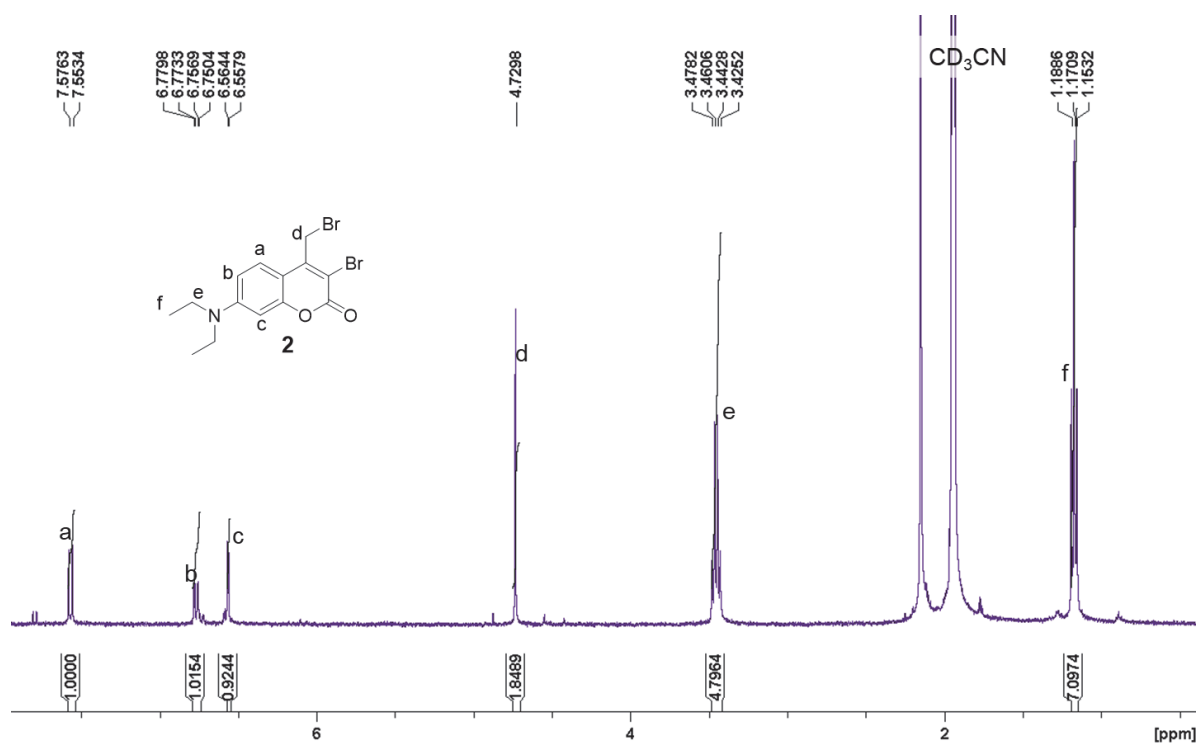


Figure 24. <sup>1</sup>H NMR of compound **2** in CD<sub>3</sub>CN.

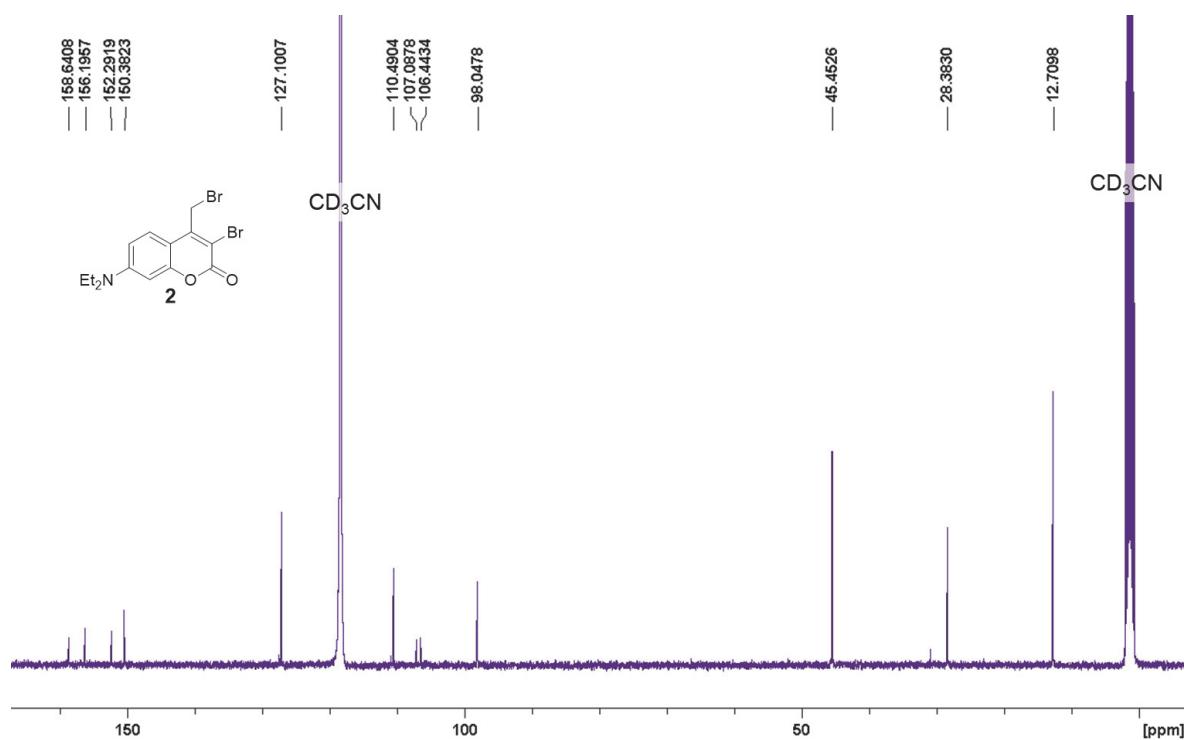


Figure 25. <sup>13</sup>C NMR of compound **2** in CD<sub>3</sub>CN.

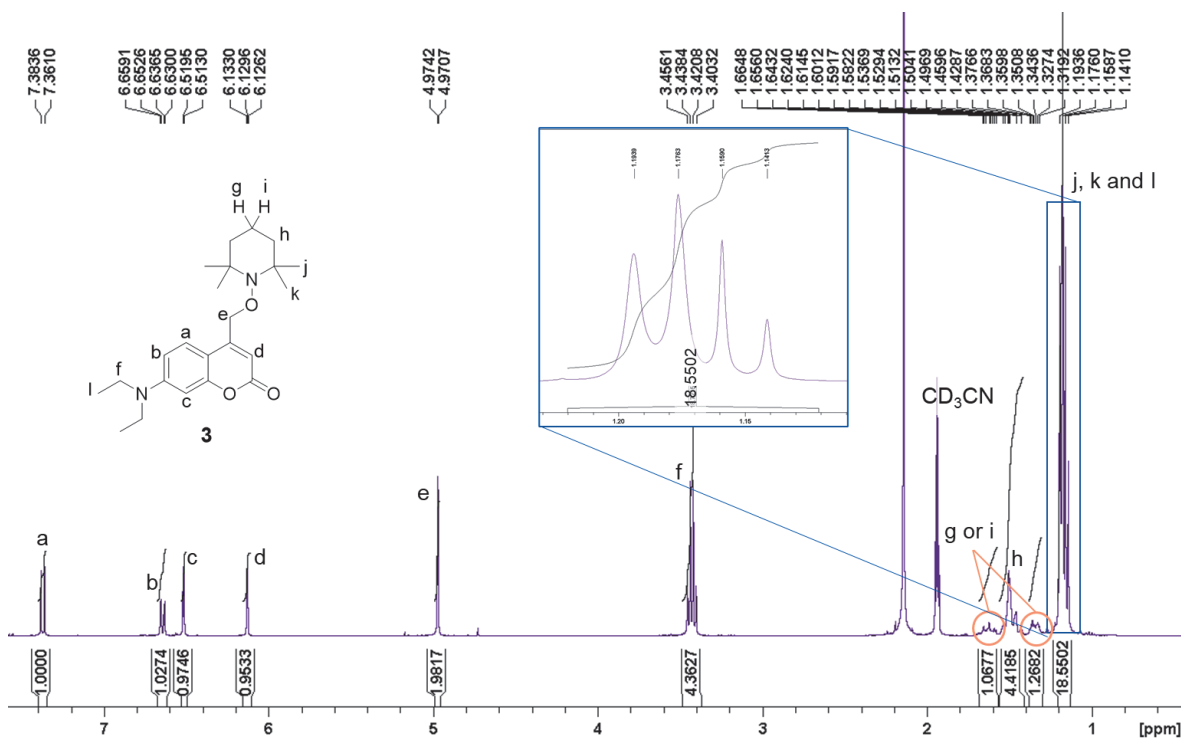


Figure 26.  $^1\text{H}$  NMR of compound 3 in  $\text{CD}_3\text{CN}$ .

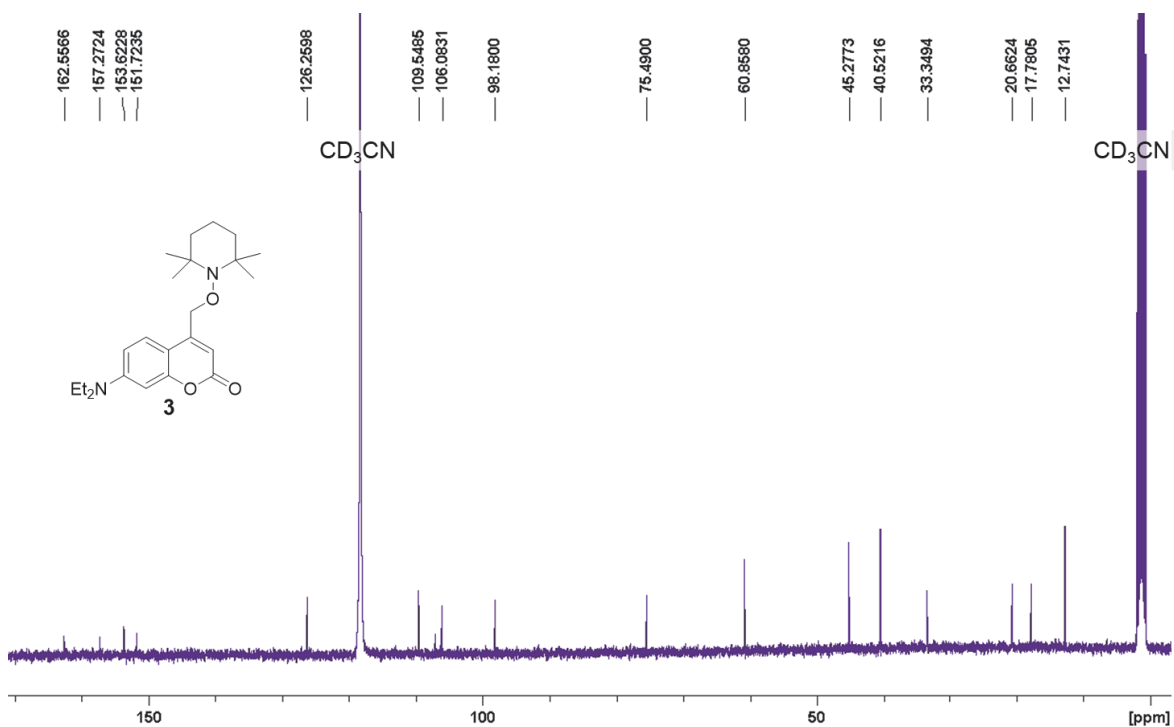
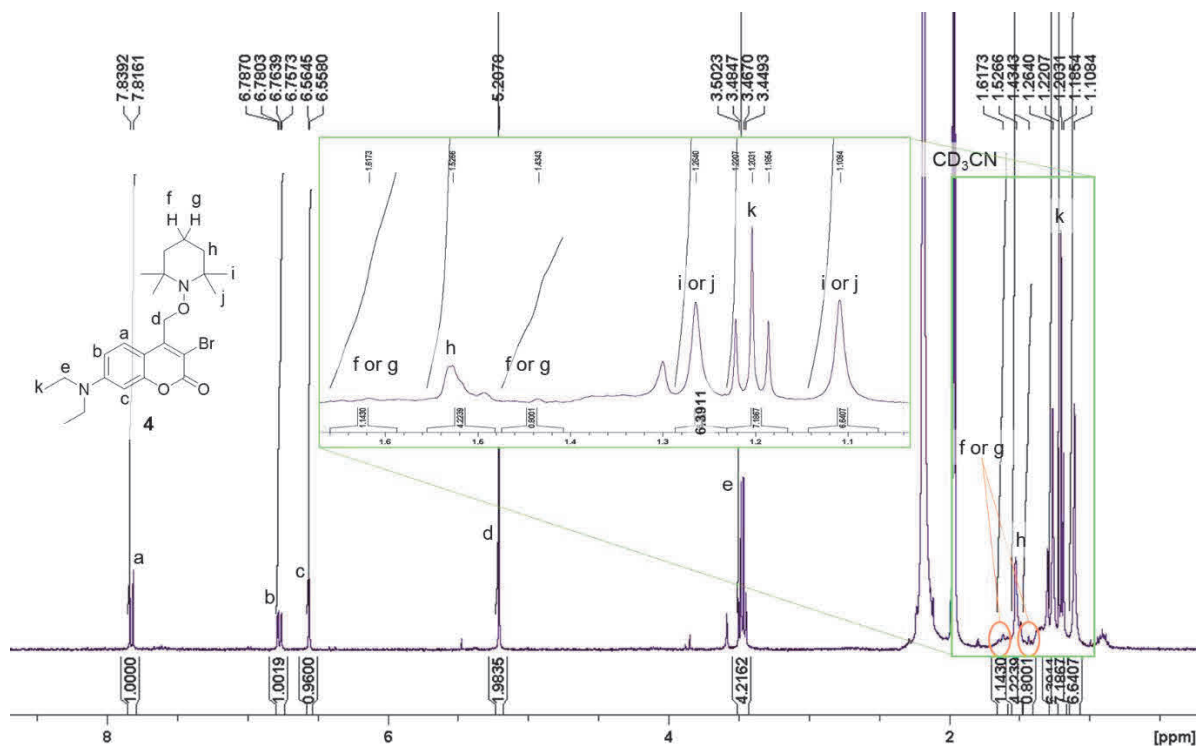
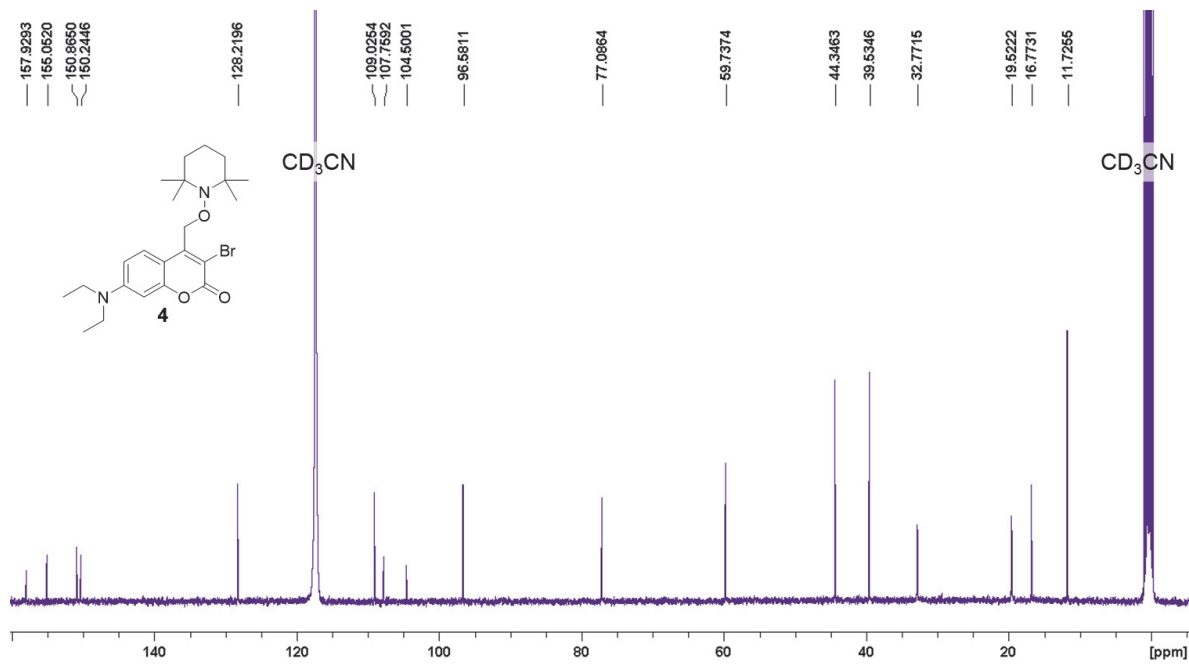


Figure 27.  $^{13}\text{C}$  NMR of compound 3 in  $\text{CD}_3\text{CN}$ .



**Figure 28.**  $^1\text{H}$  NMR of compound **4** in  $\text{CD}_3\text{CN}$ .



**Figure 29.**  $^{13}\text{C}$  NMR of compound **4** in  $\text{CD}_3\text{CN}$ .



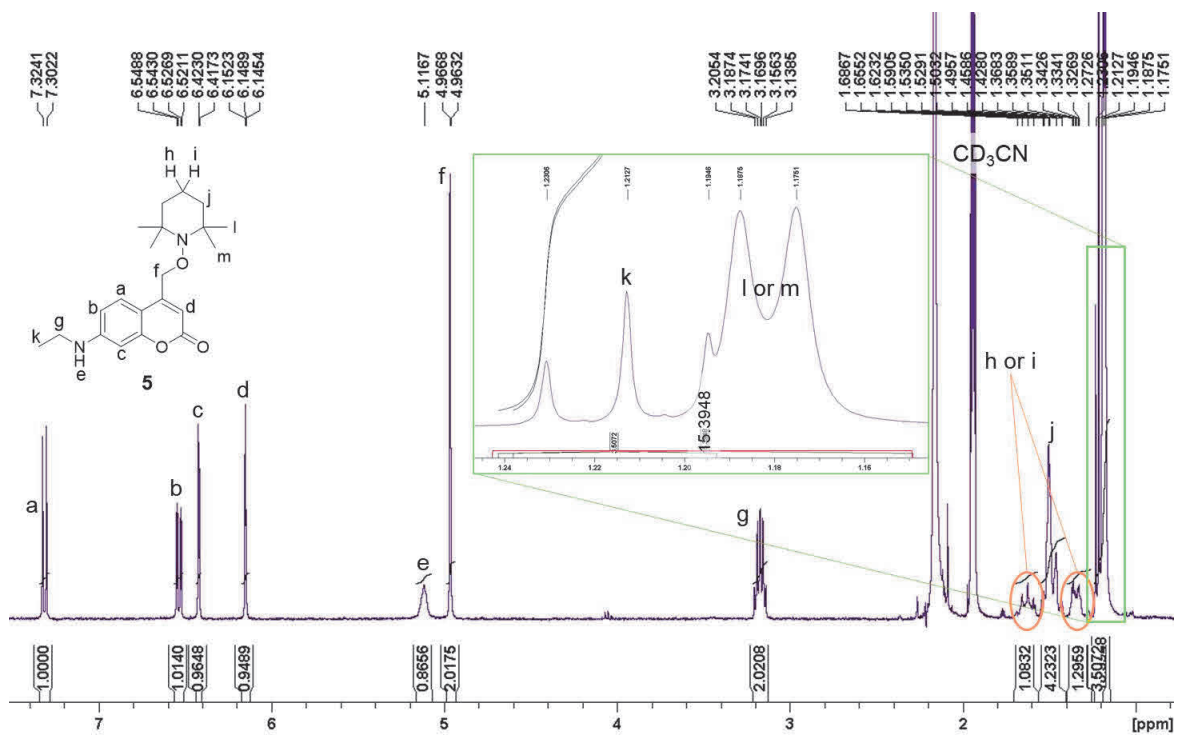


Figure 30. <sup>1</sup>H NMR of compound 5 in CD<sub>3</sub>CN.

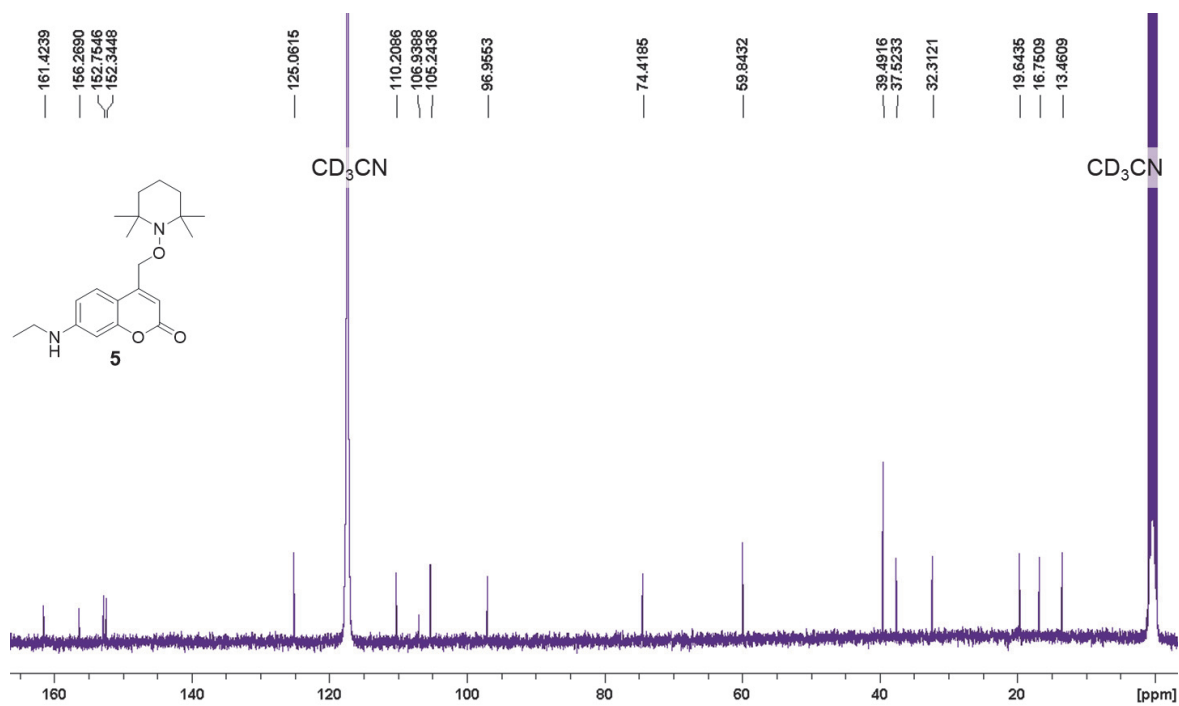


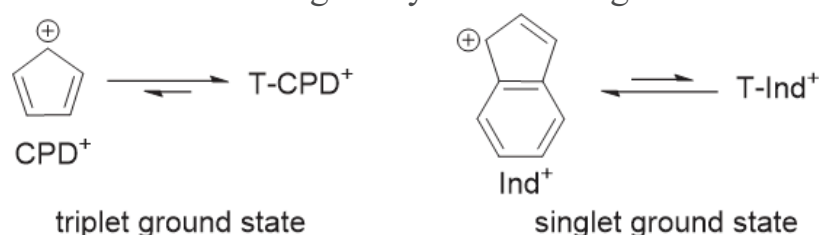
Figure 31. <sup>13</sup>C NMR of compound 5 in CD<sub>3</sub>CN.



**Chapter 3.**  
**Design of Triplet Ground State Indenyl Cation;**  
**Investigation of Substituent effects**

### 3-1. Introduction

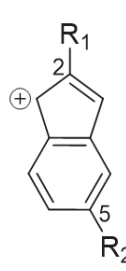
Cyclopentadienyl cation ( $\text{CPD}^+$ ) is well known as one of the triplet ground state carbocation. Due to the Hückel anti-aromaticity in closed-shell singlet (CS) and Baird aromaticity<sup>29,30</sup> in triplet (T) of  $\text{CPD}^+$ , T( $\text{T-CPD}^+$ ) is  $\Delta E_{\text{ST}} = 8.7 \text{ kcal mol}^{-1}$  more stable than singlet<sup>31-33</sup>. On the other hand, although indenyl cation ( $\text{Ind}^+$ ) which fused one benzene ring to  $\text{CPD}^+$  also have Hückel anti-aromaticity in its CS and Baird aromaticity in T, CS is ground state ( $\Delta E_{\text{ST}} \approx -9.2 \text{ kcal mol}^{-1}$ )<sup>33</sup>. The resonance stabilization of the positive charge ( $22.0 \text{ kcal mol}^{-1}$ )<sup>33</sup> by the fused benzene ring is key in stabilizing the CS state.



**Scheme 7.** Ground state of cyclopentadienyl cation ( $\text{CPD}^+$ ) and indenyl cation ( $\text{Ind}^+$ )

In this study, the substituent effect on the electronic ground state were investigated about  $\text{Ind}^+$  derivatives **7-17**(Table 6) which introduced substituent  $\text{R}_1$  and  $\text{R}_2$  at  $\text{C}_2$  and  $\text{C}_5$  of  $\text{Ind}^+$ , respectively, by density functional theory (DFT) and complete active space multiconfiguration (CAS) second order perturbation theory (CASPT2/CASSCF) calculations to demonstrate strategy for control electronic ground state of indenyl cation.

**Table 6.** Investigated cations bearing substituents ( $\text{R}_1$  and  $\text{R}_2$ ) at  $\text{C}_2$  and  $\text{C}_5$ .

	cation	$\text{R}_1$	$\text{R}_2$	cation	$\text{R}_1$	$\text{R}_2$
	<b>7</b>	H	H	<b>13</b>	$\text{NO}_2$	H
<b>8</b>	Me	H	<b>14</b>	4-MeOC <sub>6</sub> H <sub>4</sub>	H	
<b>9</b>	OMe	H	<b>15</b>	4-NO <sub>2</sub> C <sub>6</sub> H <sub>4</sub>	H	
<b>10</b>	Ph	H	<b>16</b>	4-MeOC <sub>6</sub> H <sub>4</sub>	NH <sub>2</sub>	
<b>11</b>	NH <sub>2</sub>	H	<b>17</b>	4-MeOC <sub>6</sub> H <sub>4</sub>	NO <sub>2</sub>	
<b>12</b>	CN	H				

### 3-2. Electronic structure and configuration of 7-17

Geometry optimization and vibrational analysis of CS and T of cation 7(=Ind<sup>+</sup>, R<sub>1</sub>, R<sub>2</sub> = H, H) were performed at B3LYP/6-31G(d,p) level, and the optimized structure was used for single point calculation of energy at CASPT2/cc-pVDZ level. These calculations showed singlet is 9.99 kcal mol<sup>-1</sup> (RB3LYP) or 13.1 kcal mol<sup>-1</sup> (CASPT2) more stable than triplet, and this result is well matched with literature value<sup>33</sup>. Analysis of the CASSCF reference wavefunction confirmed domination of only one leading configuration in the wavefunction for both singlet (weight 83%) and triplet (weight 84%) states. This indicates that singlet has little open-shell singlet (OS) character (Table 17). To understand electronic structure of 7, NBO charges and NBO spin densities of CS (CS-7) and T (T-7) were calculated at (R/U)B3LYP/6-31G(d,p) level (Figure 32(a)). In CS-7, positive charges are delocalized on benzyl position, C1/C3 and on the benzene ring C4/C7. On the other hand, in T-7 the positive charge at C2 is larger than that at C1/C3, and also the considerable positive charge is found at C5/C6. The spin density of T-7 at C1/C3 is higher than that at C2. From these results, introduction of substituents at C2 and C5 are predicted to most affect to stability of triplet. Thus, ground electronic state (singlet *versus* triplet) of indenyl cation 7-17 introduced the electron-donating group (EDG) or the electron-withdrawing group (EWG) at C2 or C5 were investigated by DFT and CASPT2 calculations.

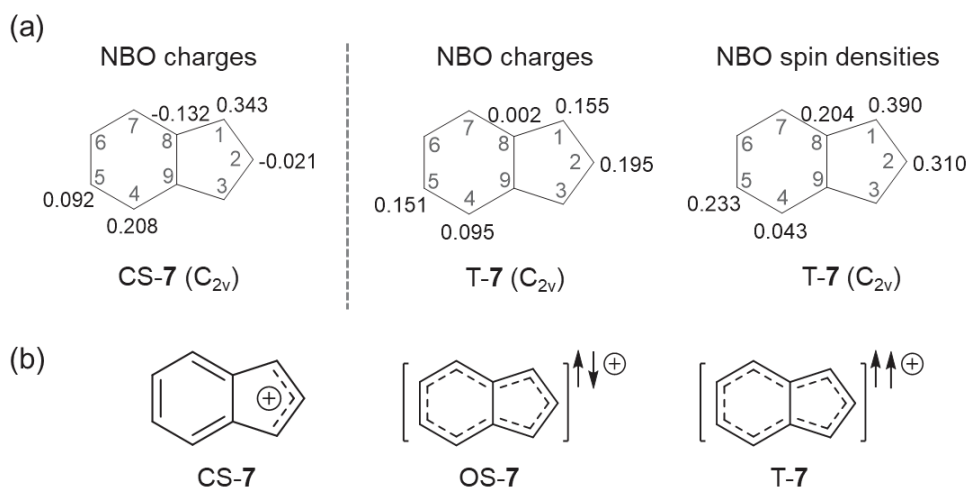


**Figure 32.** (a) NBO charges of CS-7 and NBO charges and NBO spin densities of T-7 at the (R or U)B3LYP/6-31G(d,p) level of theory; (b) typical form of CS-

7, OS-7 and T-7.

Geometries of singlet and triplet of indenyl cations **8-17** were optimized at (R or U)B3LYP/6-31G(d,p) level, and vibrational analysis was also conducted at same calculation level to confirm no imaginary frequency. The geometries and energies were re-evaluated by the broken-symmetry (BS)<sup>34-37</sup> UB3LYP/6-31G(d,p) method, resulting cations **9-11**(R<sub>1</sub>,R<sub>2</sub> = OMe,H; Ph,H; NH<sub>2</sub>,H) and **14-17**(R<sub>1</sub>,R<sub>2</sub> = 4-MeOC<sub>6</sub>H<sub>4</sub>,H; 4-NO<sub>2</sub>C<sub>6</sub>H<sub>4</sub>,H; 4-MeOC<sub>6</sub>H<sub>4</sub>,NH<sub>2</sub>; 4-MeOC<sub>6</sub>H<sub>4</sub>,NO<sub>2</sub>) has more stable OS than CS was confirmed. Single point calculations by multireference CASPT2 methods by using optimized geometries at (R or U)B3LYP/6-31G(d,p) level. Wavefunction details and natural occupation numbers of active orbitals are listed in Table 7. Distinct from parent indenyl cation **7**, almost all singlet wavefunctions of substituted derivatives has multiconfigurational character, e.g. CS configuration and OS configuration. Specifically, for cations **9**(R<sub>1</sub>,R<sub>2</sub> = OMe,H), **11**(R<sub>1</sub>,R<sub>2</sub> = NH<sub>2</sub>,H), **14**(R<sub>1</sub>,R<sub>2</sub> = 4-MeOC<sub>6</sub>H<sub>4</sub>,H), weight of leading configuration corresponds to classical HF closed-shell configuration was significantly lower than that of unsubstituted indenyl cation **7**, and contribution of second configuration (double excitation) was more than 10% (weights = 0.19, 0.12, and 0.20 for **9**, **11** and **14**, respectively). Natural occupation number of frontier orbital (1.46 and 0.55 for **9**, 1.62 and 0.41 for **11**, and 1.39 and 0.65 for **14**) was between 2 to 0 indicates singlet of these cations has diradical OS character. Whereas, in singlet of cation **8**(R<sub>1</sub>,R<sub>2</sub> = Me,H), **12**(R<sub>1</sub>,R<sub>2</sub> = CN,H), **13**(R<sub>1</sub>,R<sub>2</sub> = NO<sub>2</sub>,H) and **16**(R<sub>1</sub>,R<sub>2</sub> = 4-MeOC<sub>6</sub>H<sub>4</sub>,NH<sub>2</sub>), leading configuration occupied more than 80% same as parent indenyl cation **7** and second configuration is lower than 6%. Additionally, the results of their singlets calculated at RB3LYP and UB3LYP showed same results indicating that these cations have little OS character.

### 3-3. Singlet-Triplet energy splitting

The energy gap of singlet and triplet was determined using total electronic energies (E) including zero-point energy corrections as  $\Delta E_{RST} = \Delta E_{RS} - \Delta E_T$  and  $\Delta E_{UST} = E_{US} - E_T$ . Positive values of energy gap mean triplet is more stable. Singlet triplet energy gap were also determined by the energies calculated by

CASPT2 ( $\Delta E_{ST} = \Delta E_S - \Delta E_T$ ), and confirmed consistency with DFT calculations. Firstly, cation **8** introducing methyl group at 2-position was singlet ground state same with unsubstituted indenyl cation **7** ( $\Delta E_{RST} = \Delta E_{UST} = -5.31$  kcal mol<sup>-1</sup>). However, due to weak donor ability of Me, energy gap was smaller than that of **7** ( $\Delta E_{RST} = -9.99$  kcal mol<sup>-1</sup>). This result was confirmed on the result obtained by CASPT2 that  $\Delta E_{ST}$  of cation **8** was 3.65 kcal mol<sup>-1</sup> smaller than that of cation **7**. Additionally, in both DFT and CASPT2 calculations, cation **9-11, 14** and **17** ( $R_1, R_2 = \text{OMe, H; Ph, H; NH}_2, \text{H; 4-MeOC}_6\text{H}_4, \text{H; 4-MeOC}_6\text{H}_4, \text{NO}_2$ ) introduced strong EDG at C2 were triplet ground state. On the other hand, cation **12** ( $R_1, R_2 = \text{CN, H}$ ), **13** ( $R_1, R_2 = \text{NO}_2, \text{H}$ ) and **16** ( $R_1, R_2 = \text{4-MeOC}_6\text{H}_4, \text{NH}_2$ ) which introduced EWG at C2 and EDG at C5, respectively were singlet ground state. In the case of cation **15** ( $R_1, R_2 = \text{4-NO}_2\text{C}_6\text{H}_4, \text{H}$ ), singlet was 4.33 kcal mol<sup>-1</sup> more stable in CASPT2, but DFT calculation showed almost same energy between them. These quantum chemical calculation results suggest EDG/EWG substituents at C2/C5 are important factor for determining electronic ground state of indenyl cation derivatives as initially predicted from electronic structure of unsubstituted indenyl cation **7** such as NBO charges and NBO spin densities.

**Table 7.** Singlet-triplet energy gaps in kcal mol<sup>-1</sup> ( $\Delta E_{RST} = \text{singlet (RS) energy from RDFT} - \text{triplet (T) energy}$ ,  $\Delta E_{UST} = \text{singlet (US) energy from UDFT} - \text{T energy}$ , as calculated using DFT<sup>a</sup> and  $\Delta E_{ST} = \text{singlet energy} - \text{triplet energy}$  as calculated using CASPT2/CASSCF<sup>b</sup> methods).

cation R <sup>1</sup> , R <sup>2</sup>	$\Delta E_{RST}$ DFT	$\Delta E_{UST}$ DFT ( $\langle S^2 \rangle$ ) <sup>c</sup>	$\Delta E_{ST}$ CASPT2	ground state CASPT2
<b>7</b> (= Ind <sup>+</sup> ) H, H	-9.99	-9.99 <sup>d</sup> (0.00)	-13.14	S
<b>8</b> Me, H	-5.31	-5.31 <sup>d</sup> (0.00)	-9.49	S
<b>9</b> OMe, H	5.38	1.13 (0.96)	0.46	T

<b>10</b>		1.74		
Ph, H	5.48	(0.88)	-1.32	S
<b>11</b>		6.95		
NH <sub>2</sub> , H	13.15	(1.05)	4.66	T
<b>12</b>		-6.52 <sup>d</sup>		
CN, H	-6.52	(0.00)	-11.25	S
<b>13</b>		-11.17 <sup>d</sup>		
NO <sub>2</sub> , H	-11.17	(0.00)	-14.45	S
<b>14</b>		3.31		
4-MeOC <sub>6</sub> H <sub>4</sub> , H	9.62	(1.03)	7.37	T
<b>15</b>		0.38		
4-NO <sub>2</sub> C <sub>6</sub> H <sub>4</sub> , H	2.06	(0.70)	-4.33	S
<b>16</b>		-2.77		
4-MeOC <sub>6</sub> H <sub>4</sub> , NH <sub>2</sub>	-2.11	(0.18)	-7.65	S
<b>17</b>		3.67		
4-MeOC <sub>6</sub> H <sub>4</sub> , NO <sub>2</sub>	9.09	(1.02)	6.77	T

<sup>a</sup> The closed-shell singlet (CS) and triplet (T) states were computed at the R and UB3LYP/6-31G(d,p) levels of theory, respectively. Similar substituent effects were also found at the CAM-B3LYP,  $\omega$ B97XD, and M06-2x/6-31G(d,p) levels of theory (Table 12, 13). The open-shell (OS) singlet states were also calculated using the broken-symmetry (BS) unrestricted singlet method by including “guess=mix,always” in the keywords at the UB3LYP/6-31G(d,p) level of theory. <sup>b</sup> CASPT2/CASCF/cc-pVDZ level of theory. <sup>c</sup>  $\langle S^2 \rangle$ : expectation values of the spin operators in the BS calculations of the open-shell singlet states;  $\langle S^2 \rangle = 0$  for closed-shell singlet states;  $\langle S^2 \rangle = 1.0$  for pure open-shell singlet states;  $\langle S^2 \rangle = 2.0$  for pure triplet states. <sup>d</sup> The closed-shell singlet states ( $\langle S^2 \rangle = 0.00$ ) were obtained during the optimization of the open-shell singlet states, indicating that the closed-shell wavefunctions (RHF) are more stable than the open-shell wavefunctions (UHF).

### 3-4. Quantitative evaluation of the substituent effect

To quantitatively explain the substituent effect at C2, isodesmic reactions of singlet and triplet shown in equation (1) and (2) about cation **7-9** ( $R_1, R_2 = H, H$ ; Me, H; OMe, H) and **11-13** ( $R_1, R_2 = NH_2, H$ ; CN, H; NO<sub>2</sub>, H) were calculated at (R or U)B3LYP/6-31G(d,p). Obtained energies  $\Delta E$  were plotted as a function



of Hammett parameter ( $\sigma_{\text{para}}^+$ ,  $\Delta E$  versus  $\sigma_{\text{para}}^+$ ) (Figure 33). Positive  $\Delta E$  in equation (1) and (2) indicates products are more unstable than reactants, and negative  $\Delta E$  indicates products are more stable. The correlation coefficient ( $R^2 = 0.95$ ) and substituent constant ( $\rho = \text{slope} = 14$ ) of singlet Hammett plot (Equation (1)) was smaller than that of triplet ( $R^2 = 0.99$ ,  $\rho = 19$ ). These results support a considerably larger substituent effect in the T state compared to that in the singlet state.

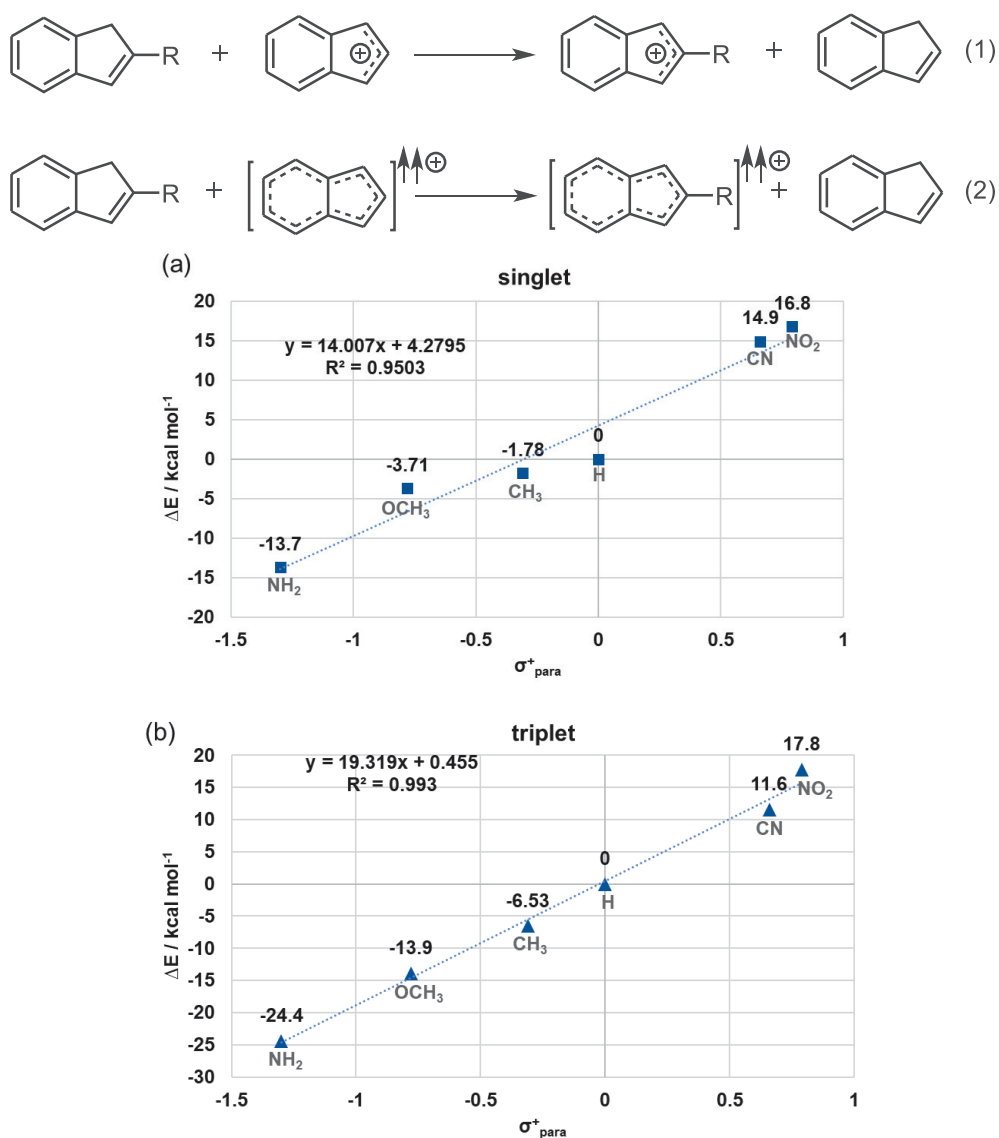
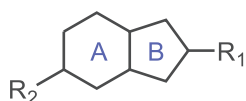


**Figure 33.** Hammett plots of the (a) singlet (Equation (1)), and (b) triplet (Equation (2))

### 3-5. Nucleus-independent chemical shift (NICS) values (NICS(1)<sub>zz</sub>)

NICS(1)<sub>zz</sub> values of six-membered ring (A) and five-membered ring (B) of CS, OS and T of cations **7-17** were calculated at (R or U) B3LYP/6-31G(d,p) level (Table 8). Positive values and negative values were obtained to singlet and T, respectively. Notably, the NICS(1)<sub>zz</sub> values of the T states are not highly dependent on the EDGs and EWGs, suggesting that the T ground state is formed via the energetic stabilization of the positive charge at the C2 position by an EDG.

**Table 8.** NICS(1)<sub>zz</sub> values of cations



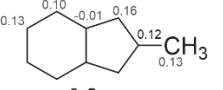
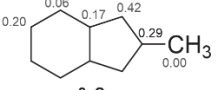
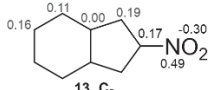
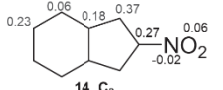
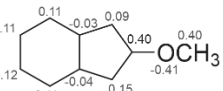
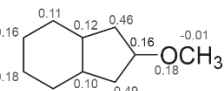
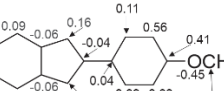
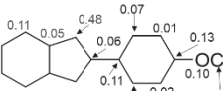
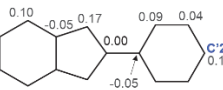
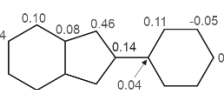
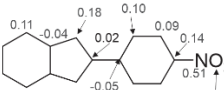
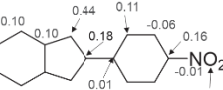
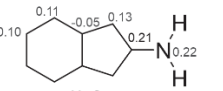
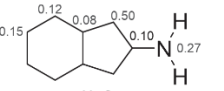
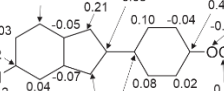
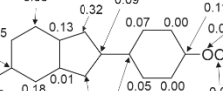
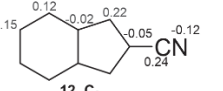
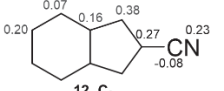
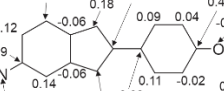
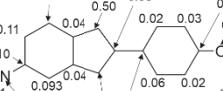
cation	R <sup>1</sup> , R <sup>2</sup>	Singlet state				Triplet state	
		RDFT		UDFT		UDFT	
		A	B	A	B	A	B
<b>7 (= Ind<sup>+</sup>)</b>	H, H	49.2	104	- <sup>a</sup>	- <sup>a</sup>	-20.7	-32.5
<b>8</b>	Me, H	59.4	121	- <sup>a</sup>	- <sup>a</sup>	-22.5	-28.8
<b>9</b>	OMe, H	144	243	50.4	98.6	-24.3	-21.9
<b>10</b>	Ph, H	165	279	41.0	89.7	-20.3	-15.3
<b>11</b>	NH <sub>2</sub> , H	1117	1608	42.4	81.0	-23.7	-18.2
<b>12</b>	CN, H	61.0	117	- <sup>a</sup>	- <sup>a</sup>	-21.3	-28.8
<b>13</b>	NO <sub>2</sub> , H	48.2	99.0	- <sup>a</sup>	- <sup>a</sup>	-19.2	-28.9
<b>14</b>	4-MeOC <sub>6</sub> H <sub>4</sub> , H	165	310	38.1	84.4	-19.3	-9.7
<b>15</b>	4-NO <sub>2</sub> C <sub>6</sub> H <sub>4</sub> , H	91.3	165	46.9	98.6	-20.3	-17.9
<b>16</b>	4-MeOC <sub>6</sub> H <sub>4</sub> , NH <sub>2</sub>	34.9	68.8	30.8	62.3	-14.5	-10.1
<b>17</b>	4-MeOC <sub>6</sub> H <sub>4</sub> , NO <sub>2</sub>	119	233	26.5	66.3	-18.5	-6.92

<sup>a</sup>same results as those obtained in the restricted and unrestricted modes

### 3-6. NBO charges and NBO spin densities

NBO charges and NBO spin densities of CS, OS and T of cation **8-17** were calculated at (R or U)B3LYP/6-31G(d,p) level shown in Table 10, 11 and 9, respectively). In T state of cation **9**(R<sub>1</sub>,R<sub>2</sub> = OMe,H) and **11**(R<sub>1</sub>,R<sub>2</sub> = NH<sub>2</sub>,H) introduced strong EDG at C2, positive charges are localized on C2. In cation **8**(R<sub>1</sub>,R<sub>2</sub> = Me,H), **12**(R<sub>1</sub>,R<sub>2</sub> = CN,H), **13**(R<sub>1</sub>,R<sub>2</sub> = NO<sub>2</sub>,H), the positive charges are localized at C1 and also delocalized to the phenyl ring of indene structure, indicating that EDG at C2 effectively stabilizes the positive charge of T state. In the T state of cation **10**(R<sub>1</sub>,R<sub>2</sub> = Ph,H), **14**(R<sub>1</sub>,R<sub>2</sub> = 4-MeOC<sub>6</sub>H<sub>4</sub>,H), **15**(R<sub>1</sub>,R<sub>2</sub> = 4-NO<sub>2</sub>C<sub>6</sub>H<sub>4</sub>,H), **16**(R<sub>1</sub>,R<sub>2</sub> = 4-MeOC<sub>6</sub>H<sub>4</sub>,NH<sub>2</sub>) and **17**(R<sub>1</sub>,R<sub>2</sub> = 4-MeOC<sub>6</sub>H<sub>4</sub>,NO<sub>2</sub>), the positive charges are mainly localized at C'2 which is para-position of the phenyl rings whereas in the singlet state, the positive charges are localized at C1 position. This indicate that the T state is selectively stabilized by resonance stabilizing effect of phenyl groups at C2 on positive charge. The relatively high spin density at C1 and C3 is confirmed in all T cations **8-17**.

**Table 9.** NBO charges and NBO spin densities of T of cation **8-17**

NBO charges of triplet	NBO spin densities of triplet	NBO charges of triplet	NBO spin densities of triplet
 <b>8, C<sub>s</sub></b>	 <b>8, C<sub>s</sub></b>	 <b>13, C<sub>2</sub></b>	 <b>14, C<sub>2</sub></b>
 <b>9, C<sub>s</sub></b>	 <b>9, C<sub>s</sub></b>	 <b>14, C<sub>s</sub></b>	 <b>14, C<sub>s</sub></b>
 <b>10, C<sub>2v</sub></b>	 <b>10, C<sub>2v</sub></b>	 <b>15, C<sub>2</sub></b>	 <b>15, C<sub>2</sub></b>
 <b>11, C<sub>2v</sub></b>	 <b>11, C<sub>2v</sub></b>	 <b>16</b>	 <b>16</b>
 <b>12, C<sub>2v</sub></b>	 <b>12, C<sub>2v</sub></b>	 <b>17</b>	 <b>17</b>

### **3-7. Conclusion**

In this study, substituent effect on electronic ground state were investigated for indenyl cation derivatives introduced substituents at C2 or C5 by DFT and CASPT2 calculations. It was found that by introducing electron donating group at C2, indenyl cation will be triplet ground state from the results of both DFT and CASPT2 calculations. Whereas, when introduce electron withdrawing group at C2, indenyl cation will be singlet ground state was suggested by CASPT2 calculations. These results can be explained by selectively stabilization of triple state by introducing substituents.

### 3-8. Supplementary information

#### • General Information

Quantum chemical computations in the gas phase have been performed with the *Gaussian* 16 (RevisionB.01) suite of programs. Charge, spin multiplicity, number of imaginary frequencies, energy (in Hartree) and Cartesian coordinates (in Å) of computed geometries at (R or U) B3LYP/6-31G(d,p) level of theory are listed in the following.

Anisotropy of the induced current density (AICD)<sup>38</sup> analyses were performed with AICD<sup>S32</sup> 3.0.4 software package. The NMR with CSGT method were calculated at (R or U) B3LYP/6-31G(d,p) level of theory. POV-Ray 3.7 on Windows was used for visualization of AICD maps.

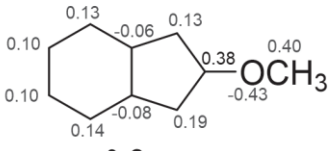
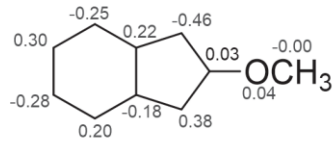
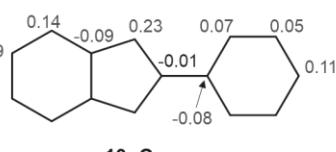
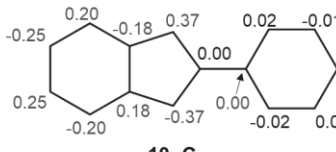
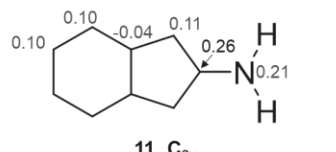
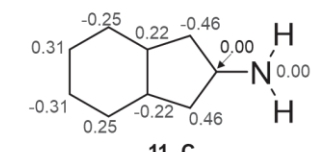
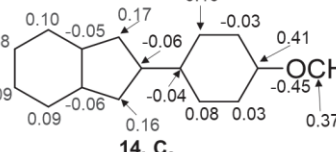
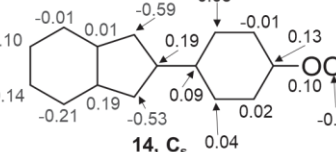
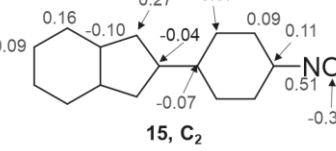
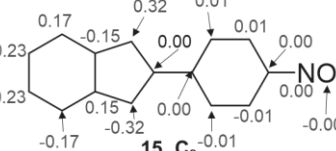
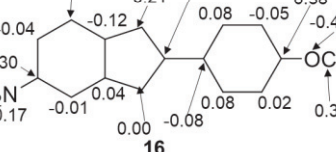
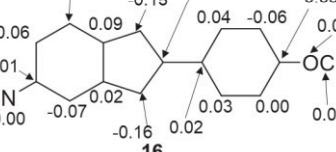
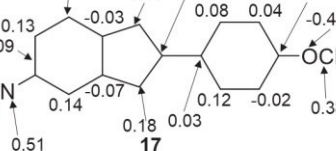
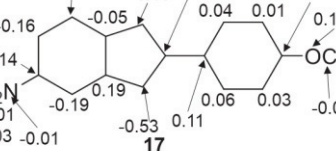
The single point CASSCF and CASPT2 calculations in conjunction with the cc-PVDZ basis set and using UB3LYP/6-31G(d,p) optimized geometries were performed by OpenMolcas programme (version 23.06)<sup>39,40</sup>

• NBO charges and spin densities

Table 10. NBO charges of singlets minimized with RB3LYP

NBO charges of singlets obtained with RB3LYP	
<p><b>8, C<sub>s</sub></b></p>	<p><b>9, C<sub>s</sub></b></p>
<p><b>10, C<sub>2v</sub></b></p>	<p><b>11, C<sub>s</sub></b></p>
<p><b>12, C<sub>2v</sub></b></p>	<p><b>13, C<sub>2v</sub></b></p>
<p><b>14, C<sub>s</sub></b></p>	<p><b>15, C<sub>2</sub></b></p>
<p><b>16</b></p>	<p><b>17</b></p>

**Table 11.** NBO charges of singlets minimized with UB3LYP

NBO charges of singlets obtained with UB3LYP	NBO spin densities of singlets obtained with UB3LYP
 <p><b>9, C<sub>s</sub></b></p>	 <p><b>9, C<sub>s</sub></b></p>
 <p><b>10, C<sub>2v</sub></b></p>	 <p><b>10, C<sub>2v</sub></b></p>
 <p><b>11, C<sub>2v</sub></b></p>	 <p><b>11, C<sub>2v</sub></b></p>
 <p><b>14, C<sub>s</sub></b></p>	 <p><b>14, C<sub>s</sub></b></p>
 <p><b>15, C<sub>2</sub></b></p>	 <p><b>15, C<sub>2</sub></b></p>
 <p><b>16</b></p>	 <p><b>16</b></p>
 <p><b>17</b></p>	 <p><b>17</b></p>

•  $\Delta E_{RST}$  and  $\Delta E_{UST}$  with different calculation level

$\Delta E_{RST}$  = singlet (RDFT) – triplet,  $\Delta E_{UST}$  = singlet (UDFT) – triplet.

**Table 12.**  $\Delta E_{RST}$  in kcal mol<sup>-1</sup> obtained by using different density functionals.

Structure number	R	B3LYP 6-31G(d,p)	CAM-B3LYP 6-31G(d,p)	$\omega$ B97xd 6-31G(d,p)	M06-2X 6-31G(d,p)
1	H	-9.73	-9.30	-10.0	-12.4
2	CH <sub>3</sub>	-4.98	-4.45	-5.22	-7.56
3	OCH <sub>3</sub>	+4.72	+6.17	+5.40	+3.38
4	C <sub>6</sub> H <sub>5</sub>	+5.25	+5.54	+4.55	+2.52
5	NH <sub>2</sub>	+12.2	+14.5	+13.6	+9.12
6	CN	-6.42	-6.98	-7.78	-0.1
7	NO <sub>2</sub>	-10.8	-10.9	-11.5	-13.7
8	4-OCH <sub>3</sub> C <sub>6</sub> H <sub>4</sub>	+9.50	+11.9	+11.6	+9.03
9	4- NO <sub>2</sub> C <sub>6</sub> H <sub>4</sub>	+2.03	+1.42	+0.0508	-1.78

**Table 13.**  $\Delta E_{UST}$  in kcal mol<sup>-1</sup> obtained by using different density functionals.

Structure number	R	B3LYP 6-31G(d,p)	CAM-B3LYP 6-31G(d,p)	$\omega$ B97xd 6-31G(d,p)	M06-2X 6-31G(d,p)
1	H	-9.73	-9.30	-10.0	-12.4
2	CH <sub>3</sub>	-5.44	-5.71	-6.02	-7.55
3	OCH <sub>3</sub>	+0.425	-0.94	-0.67	-0.216
4	C <sub>6</sub> H <sub>5</sub>	+1.05	+0.41	-0.43	-0.0113
5	NH <sub>2</sub>	+0.994	-0.59	-0.23	-2.66
6	CN	-6.42	-7.43	-7.79	-10.1
7	NO <sub>2</sub>	-10.7	-10.8	-11.5	-13.7
8	4-OCH <sub>3</sub> C <sub>6</sub> H <sub>4</sub>	+2.51	+2.86	+3.12	+2.88
9	4- NO <sub>2</sub> C <sub>6</sub> H <sub>4</sub>	-0.22	+1.42	0.060	-2.55



• **Multireference calculations**

**Table 14.** Calculations of singlet-triplet gaps ( $\Delta E_{ST}/\text{kcal mol}^{-1}$ ) for different indenyl cations using CASSCF and CASPT2 methods in conjunction with cc-pVDZ basis set. In most cases all  $\pi$  and  $\pi^*$  orbitals are included into active space (See details below).

Cation	Active space	$E_{\text{tot}}/\text{a.u.}$		$\Delta E_{ST}/\text{kcal mol}^{-1}$
		S	T	
CASSCF single point using DFT optimized geometries				
1	CAS(8,9)	-344.74360	-344.72304	-12.90
2	CAS(8,9)	-383.78880	-383.77243	-10.27
3	CAS(10,10)	-458.63277	-458.63272	-0.03
4	CAS(14,15)	-574.38648	-574.38474	-1.09
5	CAS(10,10)	-399.80807	-399.80044	-4.79
6	CAS(10,11)	-436.49013	-436.47070	-12.20
7	CAS(12,12)	-548.25256	-548.22948	-14.48
8	CAS(16,16) <sup>a</sup>	-688.27150	-688.28124	6.12
9	CAS(14,15) <sup>b</sup>	-777.87022	-777.86173	-5.32
10	CAS(14,13) <sup>c</sup>	-743.31438	-743.28368	-19.26
11	CAS(14,14) <sup>d</sup>	-891.73135	-891.73811	4.24
CASPT2 single point using CASSCF reference wavefunction				
1	CAS(8,9)	-345.76371	-345.74278	-13.14
2	CAS(8,9)	-384.95331	-384.93819	-9.49
3	CAS(10,10)	-459.97287	-459.97974	4.31
4	CAS(14,15)	-576.10358	-576.10491	0.83
5	CAS(10,10)	-400.98332	-400.99074	4.66
6	CAS(10,11)	-437.74511	-437.72719	-11.25
7	CAS(12,12)	-549.76421	-549.74118	-14.45
8	CAS(16,16) <sup>a</sup>	-690.31550	-690.33215	10.45
9	CAS(14,15) <sup>b</sup>	-780.12255	-780.11746	-3.20
10	CAS(14,13) <sup>c</sup>	-745.56625	-745.55406	-7.65
11	CAS(14,14) <sup>c</sup>	-894.32542	-894.34395	11.63

<sup>a</sup>) pseudo- $\pi$  and pseudo- $\pi^*$  on the Me group are not included in active space

<sup>b</sup>) 2  $\pi$  and 1  $\pi^*$  with lowest and highest energies on SCF level, respectively, are not included in active space

c) 3  $\pi$  and 3  $\pi^*$  with lowest and highest energies on SCF level, respectively, are not included into active space

d) 4  $\pi$  and 3  $\pi^*$  with lowest and highest energies on SCF level, respectively, are not included into active space

**Table 15.** Definition of active space in CASSCF calculations (molecule's symmetry was used wherever possible). Geometries were taken from UB3LYP/6-31G(d,p) optimisations.

Cation	CAS	State	Singlet						Triplet						
			Symm	Irep	Core	Scf	Inact.	Active	State	Symm	Irep	Core	Scf	Inact.	Active
1	CAS(8,9)	1 <sup>1</sup> A <sub>1</sub>	C <sub>2v</sub>	a <sub>1</sub>	5	15	15	0	1 <sup>3</sup> B <sub>2</sub>	C <sub>2v</sub>	a <sub>1</sub>	5	15	15	0
				b <sub>1</sub>	0	3	0	5			b <sub>1</sub>	0	3	0	5
				a <sub>2</sub>	0	1	0	4			a <sub>2</sub>	0	1	0	4
				b <sub>2</sub>	4	11	11	0			b <sub>2</sub>	4	11	11	0
2	CAS(8,9)	1 <sup>1</sup> A'	C <sub>s</sub>	a'	10	29	29	0	1 <sup>3</sup> A''	C <sub>s</sub>	a'	6	21	17	6
				a''	0	5	0	11			a''	4	13	12	4
3	CAS(10,10)	1 <sup>1</sup> A'	C <sub>s</sub>	a'	11	32	32	0	1 <sup>3</sup> A'	C <sub>s</sub>	a'	11	32	32	0
				a''	0	6	1	10			a''	0	6	1	10
4	CAS(14,15)	1 <sup>1</sup> A <sub>1</sub>	C <sub>2v</sub>	a <sub>1</sub>	9	24	24	0	1 <sup>3</sup> B <sub>2</sub>	C <sub>2v</sub>	a <sub>1</sub>	9	24	24	0
				b <sub>1</sub>	0	5	0	9			b <sub>1</sub>	0	5	0	9
				a <sub>2</sub>	0	3	0	6			a <sub>2</sub>	0	3	0	6
				b <sub>2</sub>	6	18	18	0			b <sub>2</sub>	6	18	18	0
5	CAS(10,10)	1 <sup>1</sup> A <sub>1</sub>	C <sub>2v</sub>	a <sub>1</sub>	6	17	17	0	1 <sup>3</sup> B <sub>2</sub>	C <sub>2v</sub>	a <sub>1</sub>	6	17	17	0
				b <sub>1</sub>	0	3	0	6			b <sub>1</sub>	0	3	0	6
				a <sub>2</sub>	0	2	0	4			a <sub>2</sub>	0	2	0	4
				b <sub>2</sub>	4	12	12	0			b <sub>2</sub>	4	12	12	0
6	CAS(10,11)	1 <sup>1</sup> A <sub>1</sub>	C <sub>2v</sub>	a <sub>1</sub>	7	19	19	0	1 <sup>3</sup> B <sub>2</sub>	C <sub>2v</sub>	a <sub>1</sub>	7	19	19	0
				b <sub>1</sub>	0	4	0	7			b <sub>1</sub>	0	4	0	7
				a <sub>2</sub>	0	1	0	4			a <sub>2</sub>	0	1	0	4
				b <sub>2</sub>	4	12	12	0			b <sub>2</sub>	4	12	12	0
7	CAS(12,12)	1 <sup>1</sup> A <sub>1</sub>	C <sub>2v</sub>	a <sub>1</sub>	7	20	20	0	1 <sup>3</sup> B	C <sub>2</sub>	a	7	22	20	5
				b <sub>1</sub>	0	4	0	7			b	5	19	15	7
				a <sub>2</sub>	0	2	0	5							
				b <sub>2</sub>	5	15	15	0							
8	CAS(16,16) <sup>a</sup>	1 <sup>1</sup> A'	C <sub>s</sub>	a'	17	49	49	0	1 <sup>3</sup> A'	C <sub>s</sub>	a'	17	49	49	0
				a''	0	9	1	16			a''	0	9	1	16
9	CAS(14,15) <sup>b</sup>	1 <sup>1</sup> A	C <sub>2</sub>	a	11	33	30	7	1 <sup>3</sup> B <sub>2</sub>	C <sub>2v</sub>	a <sub>1</sub>	11	30	30	0
				b	7	28	24	8			b <sub>1</sub>	0	6	2	8
											a <sub>2</sub>	0	3	0	7
											b <sub>2</sub>	7	22	22	0
10	CAS(14,13)	1 <sup>1</sup> A'	C <sub>s</sub>	a'	18	52	52	0	1 <sup>3</sup> A'	C <sub>s</sub>	a'	18	52	52	0
				a''	0	10	3	13			a''	0	10	3	13
11	CAS(14,14)	1 <sup>1</sup> A'	C <sub>s</sub>	a'	20	58	58	0	1 <sup>3</sup> A'	C <sub>s</sub>	a'	20	58	58	0
				a''	0	11	4	14			a''	0	11	4	14

pseudo- $\pi$  and pseudo- $\pi^*$  on the Me group are not included in active space

<sup>b</sup>) 2  $\pi$  and 1  $\pi^*$  with lowest and highest energies on SCF level, respectively, are not included in active space

<sup>c</sup>) 3  $\pi$  and 3  $\pi^*$  with lowest and highest energies on SCF level, respectively, are not included into active space

<sup>d)</sup> 4  $\pi$  and 3  $\pi^*$  with lowest and highest energies on SCF level, respectively, are not included into active space

**Table 16.** Active orbitals and natural occupation numbers from CASSCF/cc-pVDZ calculations

Cation	State	Active orbitals and natural occupation numbers:															
		1b <sub>1</sub>	2b <sub>1</sub>	3b <sub>1</sub>	4b <sub>1</sub>	5b <sub>1</sub>	1a <sub>2</sub>	2a <sub>2</sub>	3a <sub>2</sub>	4a <sub>2</sub>							
<b>1</b>	S	1.954	1.921	1.891	0.080	0.037	1.875	0.147	0.065	0.029							
	T	1.948	1.905	1.004	0.091	0.051	1.906	1.000	0.063	0.032							
		1a''	2a''	3a''	4a''	5a''	6a''	7a''	8a''	9a''							
<b>2</b>	S	1.953	1.917	1.877	1.884	0.153	0.083	0.068	0.035	0.030							
	T	1.951	1.907	1.002	0.090	0.045	1.905	1.002	0.067	0.032							
		2a''	3a''	4a''	5a''	6a''	7a''	8a''	9a''	10a''	11a''						
<b>3</b>	S	1.955	1.981	1.900	1.884	1.464	0.555	0.103	0.098	0.019	0.040						
	T	1.957	1.978	1.913	1.902	0.998	1.012	0.093	0.084	0.026	0.0356						
		1b <sub>1</sub>	2b <sub>1</sub>	3b <sub>1</sub>	4b <sub>1</sub>	5b <sub>1</sub>	6b <sub>1</sub>	7b <sub>1</sub>	8b <sub>1</sub>	9b <sub>1</sub>	1a <sub>2</sub>	2a <sub>2</sub>	3a <sub>2</sub>	4a <sub>2</sub>	5a <sub>2</sub>	6a <sub>2</sub>	
<b>4</b>	S	1.953	1.961	1.920	1.897	1.817	0.108	0.085	0.041	0.030	1.871	1.902	0.208	0.077	0.097	0.033	
	T	1.953	1.958	1.920	1.893	0.998	0.107	0.085	0.044	0.031	1.903	1.901	1.004	0.075	0.094	0.033	
		1b <sub>1</sub>	2b <sub>1</sub>	3b <sub>1</sub>	4b <sub>1</sub>	5b <sub>1</sub>	6b <sub>1</sub>	1a <sub>2</sub>	2a <sub>2</sub>	3a <sub>2</sub>	4a <sub>2</sub>						
<b>5</b>	S	1.957	1.942	1.888	0.409	0.099	0.039	1.904	1.619	0.099	0.044						
	T	1.969	1.956	1.908	0.995	0.097	0.035	1.900	1.015	0.089	0.037						
		1b <sub>1</sub>	2b <sub>1</sub>	3b <sub>1</sub>	4b <sub>1</sub>	5b <sub>1</sub>	6b <sub>1</sub>	7b <sub>1</sub>	1a <sub>2</sub>	2a <sub>2</sub>	3a <sub>2</sub>	4a <sub>2</sub>					
<b>6</b>	S	1.954	1.941	1.914	1.891	0.083	0.067	0.036	1.864	0.155	0.065	0.028					
	T	1.949	1.932	1.893	1.007	0.104	0.072	0.044	1.906	1.000	0.062	0.032					
		1b <sub>1</sub>	2b <sub>1</sub>	3b <sub>1</sub>	4b <sub>1</sub>	5b <sub>1</sub>	6b <sub>1</sub>	7b <sub>1</sub>	1a <sub>2</sub>	2a <sub>2</sub>	3a <sub>2</sub>	4a <sub>2</sub>	5a <sub>2</sub>				
<b>7</b>	S	1.986	1.954	1.923	1.894	0.156	0.074	0.039	1.860	1.866	0.155	0.065	0.028				
	T	1.846	1.906	1.001	0.061	0.032	1.948	1.987	1.903	1.010	0.166	0.088	0.052				
		2a''	3a''	4a''	5a''	6a''	7a''	8a''	9a''	10a''	11a''	12a''	13a''	14a''	15a''	16a''	17a''
<b>8</b>	S	1.957	1.992	1.950	1.914	1.898	1.918	1.876	1.386	0.649	0.104	0.079	0.066	0.103	0.037	0.028	0.043
	T	1.96	1.99	1.95	1.93	1.90	1.91	1.90	1.01	1.00	0.10	0.08	0.07	0.08	0.04	0.03	0.03
		31a	32a	33a	34a	35a	36a	37a	25b	26b	27b	28b	29b	30b	31b	32b	
<b>9</b>	S	1.870	1.850	1.935	0.181	0.073	0.063	0.032	1.954	1.941	1.905	1.858	0.067	0.084	0.153	0.034	
	T	1.953	1.940	1.902	1.001	0.068	0.093	0.158	0.037	1.903	1.845	1.932	1.003	0.071	0.061	0.033	
		4a''	5a''	6a''	7a''	8a''	9a''	10a''	11a''	12a''	13a''	14a''	15a''	16a''			
<b>10</b>	S	1.954	1.946	1.925	1.894	1.865	1.936	1.988	0.169	0.094	0.067	0.070	0.046	0.047			
	T	1.963	1.950	1.911	1.934	1.931	1.012	1.983	1.002	0.094	0.067	0.065	0.047	0.041			
		5a''	6a''	7a''	8a''	9a''	10a''	11a''	12a''	13a''	14a''	15a''	16a''	17a''	18a''		
<b>11</b>	S	1.952	1.935	1.850	1.884	1.917	1.785	1.922	0.267	0.072	0.147	0.077	0.099	0.055	0.038		
	T	1.958	1.940	1.850	1.928	1.931	1.923	1.009	1.007	0.081	0.151	0.059	0.070	0.054	0.037		

**Table 17.** Leading configurations<sup>a</sup> and their weights in CASSCF wavefunction for singlet and triplet states. The order of active orbitals is the same as in Table 15.

Cation	Active space	Singlet state			Triplet state		
		Leading configurations	Coeff	Weight	Leading configurations	Coeff	Weight
<b>1</b>	CAS(8,9)	22200 2000	-0.912	0.831	22u00 2u00	-0.916	0.838
		22200 0200	0.130	0.017	2uu0u 2d00	-0.107	0.012
<b>2</b>	CAS(8,9)	2222 00000	0.909	0.827	22u00 2u00	-0.917	0.841
		2u2d u0d00	0.139	0.019	2uu0u 2d00	0.108	0.012
<b>3</b>	CAS(10,10)	22222 00000	0.789	0.622	2222u u0000	0.917	0.842
		22220 20000	-0.438	0.192	22u20 20u00	-0.109	0.012
<b>4</b>	CAS(14,15)	222220000 220000	0.838	0.702	2222u0000 22u000	-0.860	0.740
		222200000 222000	-0.148	0.022			
<b>5</b>	CAS(10,10)	222000 2200	0.825	0.681	222u00 2u00	-0.912	0.832
		222200 2000	-0.346	0.120	22u000 22u0	0.108	0.012
<b>6</b>	CAS(10,11)	2222000 2000	0.894	0.799	222u000 2u00	-0.895	0.800
		2222000 0200	-0.148	0.022			
<b>7</b>	CAS(12,12)	2222000 22000	0.875	0.765	22u00 222u000	0.875	0.766
		2222200 02000	-0.236	0.056	02u00 222u200	-0.238	0.057
<b>8</b>	CAS(16,16)	22222222 00000000	-0.720	0.519	2222222u u0000000	0.869	0.754
		22222220 20000000	0.453	0.205			
<b>9</b>	CAS(14,15)	2220000 22220000	0.837	0.701	222u0000 222u000	-0.850	0.723
		2020000 22220020	-0.234	0.055	222u0020 202u000	0.240	0.058
<b>10</b>	CAS(14,13)	2222222 000000	-0.881	0.776	22222u2 u000000	-0.900	0.810
		2222022 200000	0.135	0.018			
<b>11</b>	CAS(14,14)	2222222 0000000	0.820	0.672	222222u u0000000	0.871	0.758
		2222202 2000000	-0.215	0.046	220222u u0200000	-0.243	0.059
		2202222 0020000	-0.199	0.040			

<sup>a</sup> 2- doubly occupied orbital, u – single occupied spin up, d – single occupied spin down, 0 – unoccupied orbital



**Chapter 4.**  
**Conclusions and Outlook**



## **Conclusions and Outlook**

In this study, novel electronic state carbocation which is known as important reactive intermediate in organic chemistry, triplet carbocations were investigated. (coumarin-7-diethylamino 4-yl)methyl cation was succeeded to experimentally demonstration. Additionally, as a novel triplet carbocation, it was suggested that the indenyl cation will be triplet ground state by introducing electron donating group at C2 by theoretical calculations.

Because reactive intermediate is ley for elucidation of reaction mechanism, this research can give new insights to reaction mechanistic research of organic chemistry that carbocation involved.

## References

- (1) Platz, M. S.; Moss, R. A. Reactive Intermediate Chemistry. *Wiley Intersci.* **2004**, *41*, 41-5920-41–5920. <https://doi.org/10.5860/choice.41-5920>.
- (2) Norris, F. J. On the Non-Existence of Trivalent Carbon. *Am. Chem. J.* **1901**, *25*, 117.
- (3) Kehrmann, F.; Wentzel, F. Ueber Die Basischen Eigenschaften Des Kohlenstoffs Und Die Constitution Des Sogenannten Triphenylmethyls. *Chem. Ber.* **1901**, *34*, 3815.
- (4) Olah, G. A. 100 Years of Carbocations and Their Significance in Chemistry. *J. Org. Chem.* **2001**, *66*, 5943.
- (5) Kato, T.; Reed, C. A. Putting Tert-Butyl Cation in a Bottle. *Angew. Chemie - Int. Ed.* **2004**, *43*, 2908.
- (6) Müller, T.; Juhasz, M.; Reed, C. A. The X-Ray Structure of a Vinyl Cation. *Angew. Chemie - Int. Ed.* **2004**, *43*, 1543. <https://doi.org/10.1002/anie.200352986>.
- (7) Scholz, F.; Himmel, D.; Scherer, H.; Krossing, I. Superacidic or Not? Synthesis, Characterisation, and Acidity of the Room-Temperature Ionic Liquid  $[\text{C}(\text{CH}_3)_3]^+ [\text{Al}_2\text{Br}_7]^-$ . *Chem. - A Eur. J.* **2013**, *19*, 109.
- (8) Scholz, F.; Himmel, D.; Heinemann, F. W.; V R Schleyer, P.; Meyer, K.; Krossing, I. Crystal Structure Determination of the Nonclassical 2-Norbornyl Cation. *Science.* **2013**, *341*, 62.
- (9) McClelland, R. A.; Banait, N.; Steenken, S. Electrophilic Reactivity of the Triphenylmethyl Carbocation in Aqueous Solutions. *J. Am. Chem. Soc.* **1986**, *108*, 7023.
- (10) Pople, J. A. The Non-Planar Structure of the Triplet Methyl Cation. *Chem. Phys. Lett.* **1982**, *91*, 9.
- (11) Dill, D. J.; Schleyer, R. v. P.; Pople, J. A. Ab Initio Studies of Aminophenyl Cations. *Tetrahedron Lett.* **1975**, 2857.
- (12) Dill, J. D.; Schleyer, P. R.; Pople, J. A. Molecular Orbital Theory of the Electronic Structure of Molecules. 31. Substituent Stabilization of the Phenyl Cation. *J. Am. Chem. Soc.* **1977**, *99*, 1.
- (13) Guizzardi, B.; Mella, M.; Fagnoni, M.; Freccero, M.; Albini, A. Generation and Reactivity of the 4-Aminophenyl Cation by Photolysis of 4-Chloroaniline. *J. Org. Chem.* **2001**, *66*, 6353.
- (14) Winter, A. H.; Falvey, D. E. Vinyl Cations Substituted with  $\pi$ -Donors Have Triplet Ground States. *J. Am. Chem. Soc.* **2010**, *132*, 215.

- (15) Winter, A. H.; Falvey, D. E.; Cramer, C. J.; Gherman, B. F. Benzylic Cations with Triplet Ground States: Computational Studies of Aryl Carbenium Ions, Silylenium Ions, Nitrenium Ions, and Oxenium Ions Substituted with Meta  $\pi$  Donors. *J. Am. Chem. Soc.* **2007**, *129*, 10113.
- (16) Perrotta, R. R.; Winter, A. H.; Falvey, D. E. Photochemical Heterolysis of 3,5-Bis(Dimethylamino)Benzyl Alcohols and Esters: Generation of a Benzyl Cation with a Low-Energy Triplet State. *Org. Lett.* **2011**, *13*, 212.
- (17) Winter, A. H.; Falvey, D. E.; Cramer, C. J. Effect of Meta Electron-Donating Groups on the Electronic Structure of Substituted Phenyl Nitrenium Ions. *J. Am. Chem. Soc.* **2004**, *126*, 9661.
- (18) Y. Qiu, L. Du, S. Cady, D. L. Phillips, A. H. Winter, *ChemRxiv*. preprint **2023**, DOI: <https://doi.org/10.26434/chemrxiv-2023-k6wbl>.
- (19) Li, M. De; Albright, T. R.; Hanway, P. J.; Liu, M.; Lan, X.; Li, S.; Peterson, J.; Winter, A. H.; Phillips, D. L. Direct Spectroscopic Detection and EPR Investigation of a Ground State Triplet Phenyl Oxenium Ion. *J. Am. Chem. Soc.* **2015**, *137*, 10391.
- (20) Albright, T. R.; Winter, A. H. A Fine Line Separates Carbocations from Diradical Ions in Donor-Unconjugated Cations. *J. Am. Chem. Soc.* **2015**, *137*, 3402.
- (21) Weinrich, T.; Gränz, M.; Grünewald, C.; Prisner, T. F.; Göbel, M. W. Synthesis of a Cytidine Phosphoramidite with Protected Nitroxide Spin Label for EPR Experiments with RNA. *Eur. J. Org. Chem.* **2017**, 491.
- (22) Rane, V.; Das, R. Distance Dependence of Electron Spin Polarization during Photophysical Quenching of Excited Naphthalene by TEMPO Radical. *J. Phys. Chem. A* **2015**, *119*, 5515.
- (23) Baciocchi, E.; Del Giacco, T.; Lanzalunga, O.; Lapi, A.; Raponi, D. The Singlet Oxygen Oxidation of Chlorpromazine and Some Phenothiazine Derivatives. Products and Reaction Mechanisms. *J. Org. Chem.* **2007**, *72*, 5912.
- (24) Baciocchi, E.; Del Giacco, T.; Lapi, A. Oxygenation of Benzyldimethylamine by Singlet Oxygen. Products and Mechanism. *Org. Lett.* **2004**, *6*, 4791.
- (25) Griller, D. Oxidation Potentials of  $\alpha$ -Aminoalkyl Radicals: Bond Dissociation Energies for Related Radical Cations. *Chem. Phys. Lett.* **1986**, *131*, 189.
- (26) Bartling, H.; Eisenhofer, A.; König, B.; Gschwind, R. M. The Photocatalyzed Aza-Henry Reaction of N-Aryltetrahydroisoquinolines: Comprehensive Mechanism,  $H^\bullet$ - versus  $H^+$ -Abstraction, and Background Reactions. *J. Am.*

- Chem. Soc.* **2016**, *138*, 11860.
- (27) Zhang, X.; Seek, S. Y.; Mauro, H.; Angelo, F.; Falvey, D. E.; Mariano, P. S. Dynamics of  $\alpha$ -CH Deprotonation and  $\alpha$ -Desilylation Reactions of Tertiary Amine Cation Radicals. *J. Am. Chem. Soc.* **1994**, *116*, 4211.
- (28) Roth, H. G.; Romero, N. A.; Nicewicz, D. A. Experimental and Calculated Electrochemical Potentials of Common Organic Molecules for Applications to Single-Electron Redox Chemistry. *Synlett* **2016**, *27*, 714.
- (29) Baird, C. N. *J. Am. Chem. Soc.* **1971**, *53*, 4941.
- (30) Ottosson, H. Exciting Excited-State Aromaticity. *Nat. Chem.* **2012**, *4*, 969.
- (31) Breslow, R.; Chang, W.; Hill, R.; Wasserman, E. Stable Triplet States of Some Cyclopentadienyl Cations. *J. Am. Chem. Soc.* **1967**, *89*, 1112.
- (32) Saunders, M.; Berger, R.; Jaffe, A.; McBride, J. M.; O'Neill, J.; Breslow, R.; Hoffmann, J. M.; Perchonock, C. Jr.; Wasserman, E.; Hutton, S. R.; Kuck, J. V. Unsubstituted Cyclopentadienyl Cation, a Ground-State Triplet. *J. Am. Chem. Soc.* **1973**, *95*, 3017.
- (33) Jiao, H.; Von Ragué Schleyer, P.; Mo, Y.; McAllister, M. A.; Tidwell, T. T. Magnetic Evidence for the Aromaticity and Antiaromaticity of Charged Fluorenyl, Indenyl, and Cyclopentadienyl Systems. *J. Am. Chem. Soc.* **1997**, *119*, 7075.
- (34) Noodleman, L. Valence Bond Description of Antiferromagnetic Coupling in Transition Metal Dimers. *J. Chem. Phys.* **1981**, *74*, 5737.
- (35) Baerends, E. J.; Noodleman, L. Electronic Structure, Magnetic Properties, ESR, and Optical Spectra for 2-Fe Ferredoxin Models by LCAO-X $\alpha$  Valence Bond Theory. *J. Am. Chem. Soc.* **1984**, *106*, 2316.
- (36) Kizashi, Y.; Takahara, Y.; Fueno, T.; Nasu, K. Ab Initio MO Calculations of Effective Exchange Integrals between Transition-Metal Ions via Oxygen Dianions: Nature of the Copper-Oxygen Bonds and Superconductivity. **1987**, p L1362.
- (37) Yamaguchi, K.; Jensen, F.; Dorigo, A.; Houk, K. N. A Spin Correction Procedure for Unrestricted Hartree-Fock and Møller-Plesset Wavefunctions for Singlet Diradicals and Polyradicals. *Chem. Phys. Lett.* **1988**, *149*, 537.
- (38) Geuenich, D.; Hess, K.; Köhler, F.; Herges, R. Anisotropy of the Induced Current Density (ACID), a General Method to Quantify and Visualize Electronic Delocalization. *Chem. Rev.* **2005**, *105*, 3758.
- (39) Vacher, M.; Alavi, A.; Angeli, C.; Aquilante, F.; Fdez, I.; Autschbach, J.; Bao, J. J.; Bokarev, S. I.; Bogdanov, N. A.; Carlson, R. K.; Delcey, G.; Dong, S. S.;

- Chibotaru, L. F.; Creutzberg, J.; Dattani, N.; Dreuw, A.; Freitag, L.; Frutos, L. M.; Gagliardi, L.; Giussani, A.; Gonza, L.; Grell, G.; Guo, M.; Hoyer, C. E.; Ka, E.; Johansson, M.; Keller, S.; Knecht, S.; Kovac, G.; Malhado, P.; Manni, G. L.; Lundberg, M.; Ma, Y.; Mai, S.; Olivucci, M.; Oppel, M.; Phung, Q. M.; Pierloot, K.; Plasser, F.; Reiher, M.; Sand, A. M.; Schapiro, I.; Sharma, P.; Stein, C. J.; Sørensen, L. K.; Truhlar, D. G.; Ugandi, M.; Ungur, L.; Valentini, A.; Vancoillie, S.; Veryazov, V.; Weser, O.; Weso, T. A.; Widmark, P.; Wouters, S.; Zech, A.; Zobel, J. P.; Lindh, R. OpenMolcas : From Source Code to Insight. *J. Chem. Theory Comput.* **2019**, *15*, 5925.
- (40) Aquilante, F.; Autschbach, J.; Baiardi, A.; Battaglia, S.; Borin, V. A.; Chibotaru, L. F.; Conti, I.; Vico, L. De; Delcey, M.; Galván, I. F.; Ferré, N.; Freitag, L.; Garavelli, M.; Gong, X.; Knecht, S.; Larsson, E. D.; Lindh, R.; Lundberg, M.; Malmqvist, P. Å.; Nenov, A.; Norell, J.; Odelius, M.; Olivucci, M.; Pedersen, T. B.; Pedraza-gonzález, L.; Phung, Q. M.; Pierloot, K.; Reiher, M.; Schapiro, I.; Segarra-martí, J.; Segatta, F.; Seijo, L.; Sen, S.; Sergentu, D.; Stein, C. J.; Ungur, L.; Vacher, M.; Valentini, A.; Veryazov, V.; Conti, I.; Galván, I. F.; Ferré, N.; Freitag, L.; Garavelli, M.; Knecht, S.; Larsson, E. D.; Lindh, R.; Lundberg, M. Modern Quantum Chemistry with [Open]Molcas. *J. Chem. Phys.* **2020**, *152*, 214117.

## **List of Publications**

## 公表論文

(1) “Photoreaction of 4-(Bromomethyl)-7-(diethylamino)coumarin: Generation of a Radical and Cation Triplet Diradical during the C-Br Bond Cleavage”

Ma-aya Takano and Manabu Abe\*

*Organic Letter.* **2022**, *24*, 2804-2808.

(2) “Substituent Effects on the Electronic Ground State (Singlet versus Triplet) of Indenyl Cations: DFT and CASPT2 Studies

Ma-aya Takano, Ivana Antol and Manabu Abe\*

*European Journal of Organic Chemistry.* **2024**. doi; 10.1002/ejoc.202301226



## **Acknowledgement**

All the research works described in this dissertation have been carried out under the guidance of Professor Manabu Abe at the Department of Chemistry, Graduate School of Advanced Science and Engineering, Hiroshima University. My research work was supported by JST, the establishment of university fellowships towards the creation of science technology innovation, Grant Number JPMJFS2129.

First and foremost, I am extremely grateful to my supervisor, Professor Manabu Abe for his invaluable advice, continuous support, and patience during my Ph.D. study. I would also like to thank Lecturer Sayaka Hatano and Assistant Professor Ryukichi Takagi for their technical support and discussion on my study. I would like to thank all the members of our laboratory. It is their kind help and support that have made my research study in an excellent time. I also thank N-BARD, Hiroshima University, for providing the EPR measurement facilities and for assistance with the MS measurements.

Finally, I would like to express my gratitude to my family for their kindness and support.

**Ma-aya Takano**

Research group of Reaction Organic Chemistry,  
Department of Chemistry,  
Graduate School of Advanced Science and Engineering,  
Hiroshima University  
February 2024